Chapter 2

Palm Shell extract capped silver nanoparticles-SERS detection and Catalytic Degradation of Dyes

2.1 Introduction

Metallic nanoparticles have attracted due to their unique optoelectronic and physico-chemical properties as well as their wide applications in bio sensing [1], media recording [2], optics [3], catalysis [4] and environmental remediation [5-10]. The diverse optical properties are mainly due to their localized surface plasmon, which results in enhanced Raman signals of molecules adsorbed on their surface, when excited by irradiation with light, termed as Surface Enhanced Raman Scattering (SERS). SERS is emerging as a popular probing technique for environmental pollutants due to its high sensitivity.

Spectroscopic studies using monomolecular layers employing SERS has been attempted by many researchers since the first discovery of anomalous increase of Raman signal from molecules adsorbed on roughened metal surfaces [11-13]. Nie and Emory reported for the first time the single molecular level detection of SERS response from fluorescent molecules adsorbed on random aggregates of metal nanoparticles [14] and since then, investigations on the enhancement of the Raman signals from various nano sized structures have been reported by many researchers [15–20]. Since the Raman scattering is due to changes in induced polarizabilities of the molecules, it can be used for detection of all types of molecules. SERS originates from electromagnetic field enhancement due to the surface plasmon resonance, the resonance Raman effect arising from the charge transfer in the metal–molecule complex [21]. Since the resonance Raman Effect depends upon the structures of the metal–molecule complex, relative enhancement of the SERS signal from certain vibrational modes would provide information on orientation as well as interaction of the adsorbed molecules relative to the metal surfaces. On the other hand, the maximum SERS signal can be observed from aggregates as SERS substrates, especially from junctions between two or more particles [22]. Wang and co workers showed an enormous enhancement of the Raman signal using size-controlled Ag nanoparticles with 5 nm gap grown inporous anodized aluminum oxide nanochannels with various sizes and gaps [23]. However, in heterogeneously aggregated colloidal nanoparticles, only a very small portion of the aggregated showed SERS activity [24,

25]. In many studies, it was found that aggregates of particles of certain sizes, termed "hot-spots" are essential to show SERS activity, although the mechanism of enhancement of the Raman signal from these hot-spots is not yet clear. These hot spots which cannot be controlled in shape and size and are random in solution result in poor reproducibility in the SERS experiments. This has resulted in efforts to synthesize colloidal solution of nanoparticles with stable, uniformly distributed hot-spots. Roughened metal surfaces and colloidal nanoparticles for SERS substrates have been generated by chemical or electrochemical reduction of metal ions in solution and direct ablation from metals by incidence of intense laser lights [26–28].

Nanoparticles of gold, platinum and silver are also of particular interest as catalysts in various organic and inorganic reactions as well as degradation of dyes. However, the chemical methods involved in the synthesis of nanomaterials generate a large amount of hazardous by products, necessitating green synthetic techniques [29]. Several nanoparticles (NPs), such as Ag [29-31], Au [32], Pd [33,34], $CaCO_3$[35,36], $BaCO_3$[36], $SrCO_3$[37], ZrO_2[38], TiO_2 [39], SiO_2 [39,40], $CdCO_3$ [41] $BaTiO_3$ [42,43], Fe_3O_4 [44], $CuAlO_2$ [45] CdS [46, 47] and Sb_2O_3 [48] have been synthesized using micro-organisms. Recently, plant extracts, and plant biomass are emerging as alternative sources for the synthesis of metal NPs [49, 50]. For instance, alfalfa [51], broths of geranium [52], neem [53] and Emblica Officinalis fruit [54] as well as Aloe vera leaves [55], extracts of Chlorella vulgaris [56], Capsicum Annuum L.[57], coffee and Tea [58], Camellia Sinensis [59], Eclipta leaf [60] Azadirachtaindica leaf [61], Sundried Cinnamonum and camphora leaf [62, 63] have been used to prepare Ag nanoparticles (AgNPs). Fruit peel extracts have also been used for the synthesis of AgNPs. These extracts are reportedly known to function as both reducing and stabilizing agents during the synthesis of AgNPs. However to the best of our knowledge there are no reports of synthesis of nanoparticles using shells of any fruits.

Borassus Flabellifer (Palm tree) is well known and widely distributed in India. Previous studies have revealed that palm shell has good complexation and reducing properties attributed to abundant hydroxyl, carbonyl and carboxyl groups present in it [64, 65]. Hence we felt that an attempt could be made to use palm shell extract for the synthesis and stabilization of nanoparticles.

Degradation of dyes through advanced oxidation processes using H_2O_2 has emerged as a promising technique as the oxidation reaction can be performed at ambient conditions. The degradation mechanism is based on the generation of

hydroxyl and superoxide radicals, which are able to mineralize the dyes in waste water. Infact, AgNPs are known to catalyze the decomposition of H_2O_2 wherein superoxide is produced following the oxidation of AgNPs by H_2O_2. We felt that the radicals formed during the oxidation of AgNPs by H_2O_2 which is already present in textile effluents as mentioned in chapter 1 could be used for the degradation of dyes. It was felt that the ability for AgNPs to undergo catalytic cycling could provide a pathway for the continual generation of Reactive Oxygen Species, degradation of dyes and the regeneration of AgNPs following oxidation.

2.1.1 Materials and methods

Silver nitrate (Merck, 99.9%), 4-nitrophenol (extrapure AR); commercially used dyes Reactive blue-21(RB-21), Reactive red-141, Rhodamine-6G (Rh-6G), hydrogen peroxide (H_2O_2, Fisher Scientific; 30%solution), were used in this study without further purification. Palm shells obtained from the coastal areas of Andhra Pradesh, India; were washed, sun dried for 24 h and ground using a jaw crusher. They were then dried at 110℃ and used for preparation of extract. The structures of dyes used are presented in table 2.1.

Table 2.1 Structure of dyes

Name	Structure
Reactive blue -21	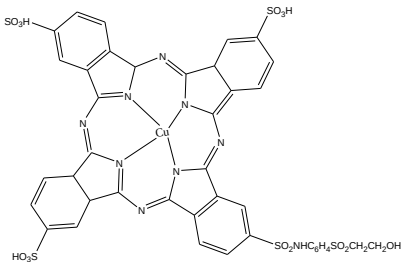
Reactive red-141	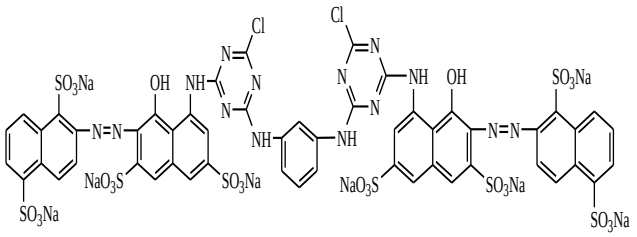
Rhodamine 6G	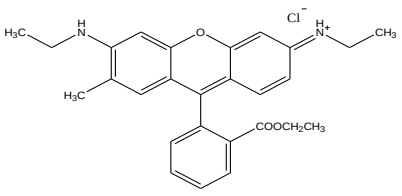

2.1.2 Synthesis of palm shell extract, silver nanoparticles

Preparations of Palm shell extract (PS)

About 40 g of powdered palm shell powder was soxhleted using 300 mL of deionized water at80^{o}Cfor 10 h. The extracts were concentrated and the resultant extract solution was refrigerated and stored for further use.

Synthesis of Silver nanoparticles (AgPS)

Silver nanoparticles were prepared by adding 0.1M $AgNO_3$ solution to palm shell extract in a 2:1 volume ratio. The mixture was shaken for 1 min. The solution turned yellow indicating the formation of silver nanoparticles (AgPS) and then brown after few minutes. The solution was kept standing for 6h for the stabilisation of silver nano particles based on UV experiments discussed in section 2.2.2

2.1.3 Characterisation of the synthesised materials

The UV-visible spectra of the solution were recorded using a Perkin Elmer Lambda-35 spectrophotometer. The dried nanoparticles were used for powder X-ray diffraction (XRD) analysis. The spectra were recorded using a Bruker D8 Advance powder diffractometer operating in the reflection mode with CuKα radiation. The diffracted intensities were recorded from 20° to 80°. TEM images were recorded using Philips (Model CM200) transmission electron microscope. EDS analysis was done using a SEM/EDX (JEOL, model JSM-5610LV) microscope operating at 200 kV. FTIR spectra were collected using Perkin Elmer RX1model within the wavenumber range 400 – 4000 cm^{-1}. The Raman spectra of dyes (Rh6G, RB21 and RR141) as well as AgPS were obtained using Horiba LabRAM HR Raman & PL instrument equipped with 514nm LASER and CCD detector. SERS measurements were done by depositing the dyes onto AgPS substrate. Drops (10μL of 100 ppm) of the dye were deposited onto 0.5 mg AgPS, allowed to dry and then examined. Zeta potential was measured using Brookhaven instruments 90plus/BI-MAS. TOC analysis of the degraded dye solution was done using a Shimadzu make TOC analyser

2.1.4 Dye degradation experiments

The dye solution (100 ppm) was prepared by dissolving the required amount of dye in Double Distilled Water. Samples were prepared by mixing 3 mL of the dye solution, 200 μL of 30%H_2O_2 in the cuvette and 0.5 mg catalyst was added to the solution and quickly mixed. Scans were started immediately after the addition of nanoparticles, and the solution was left untouched until completion. Absorbance was monitored at the wavelength of maximum absorption of the respective dyes.

Degradation experiments for binary mixtures (100 ppm+100 ppm) were performed by following a similar procedure as for single dyes. Measurements were carried out at the maximum absorbance wavelength of the mixture of dyes under investigation.

2.1.5 Catalytic reduction of 4-nitrophenol(4 NP)

The potential of AgPS as a catalyst was further tested by investigating the reduction of 4-nitrophenol(4-NP). About 1.5 mL of water, 0.3 mL of 2 mM solution of 4-NP, and 1mL of 0.01M $NaBH_4$ solution were mixed in a 3 mL standard quartz cuvette. To this reaction mixture, 0.3 mg of catalyst was added for further reaction to proceed. After complete reduction, the catalyst was filtered out and washed for the next cycle.

2.2 Results and discussions

2.2.1 Zeta potential analysis

The effect of pH on the zeta potential of silver nanoparticles was investigated(Figure 2.1). TheAgPS particles are seen to be positively charged only at pH 1 and negatively charged from pH 2-11.The stability could be attributed to the high negative zeta potential value of -41.91mv for the nanoparticles.

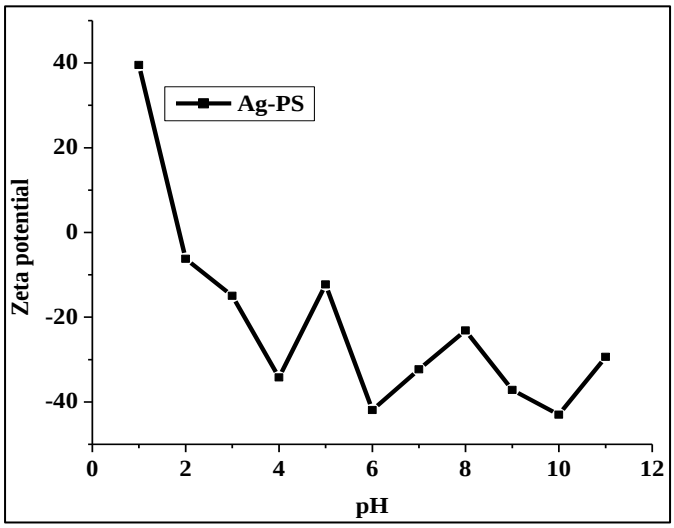

Figure 2.1 Zeta potential spectra of AgPS

2.2.2 UV-Vis Absorption Spectroscopy

The time resolved UV-Vis spectra are shown in Figure 2.2. The UV-VIS spectra of the colloidal silver nanoparticles showed an intense surface plasmon resonance (SPR) peak at 446 nm. According to Mie's theory, only a single SPR band is expected in the absorption spectra of spherical nanoparticles, whereas anisotropic particles could give rise to two or more SPR bands depending on the shape of the particles. The number of SPR peaks increases as the symmetry of the nanoparticle

decreases [66]. However the broad band for AgPS indicates the formation of varied size and shape nanoparticles. The solutions of AgPS were initially yellow in colour which turned to brown after few min and was kept for 330 min for stabilisation. The optimum pH for the formation of AgPS was found to bepH6. Nanoparticle formation was not observed at acidic and basic pH (figure not shown). The absorbance spectra of silver nanoparticles showed hardly any change in the λ_{max} and intensity values, even after one month of storage. This observation is further supported by the complete absence of peaks at 335 and 560nm in UV–vis absorption spectra, indicating no nanoparticle aggregation or nanocluster formation (Figure 2.2) [67, 68].

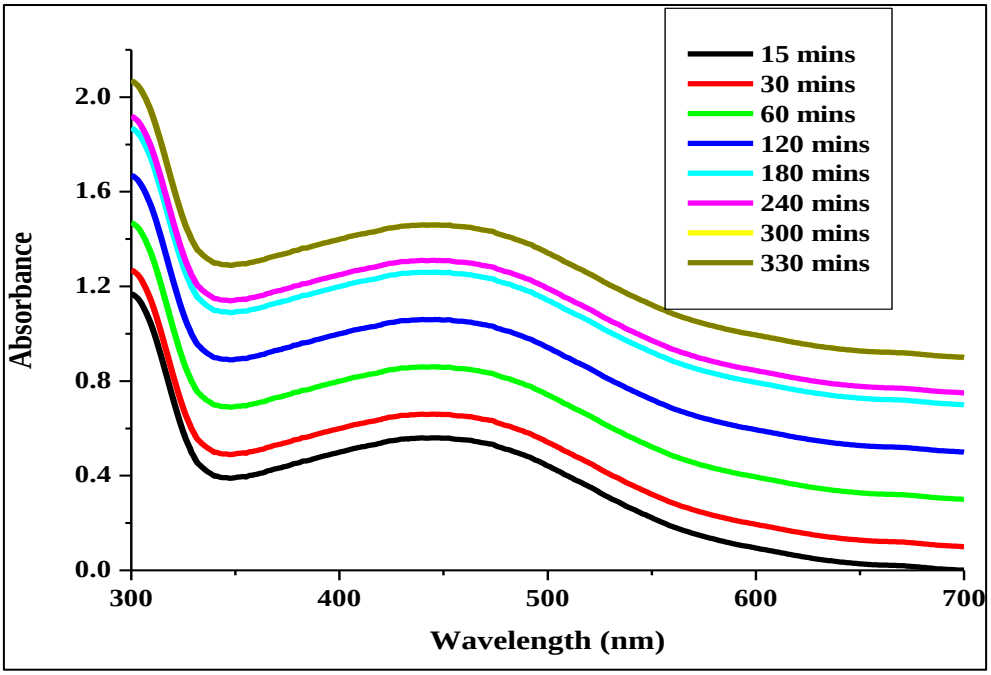

Optimum parameters pH=6, Room Temperature [RT], 0.1 N $AgNO_3$ solution

Figure 2.2 Uv-Vis spectra of the synthesised silver nanoparticles using palm shell extract

2.2.3 Morphology of Nanosilver

Figure 2.3 a & b shows the transmission electron microscope micrograph and the EDS images of silver nanoparticle clusters stabilised with AgPS [69,70].It was observed that AgPS were not uniform in shape but were with an average diameter of about 50 nm. These AgPS were found to be stable in aqueous solution over a period of about a month. TheEDS analysis confirms the presence of Ag in the nanoparticle

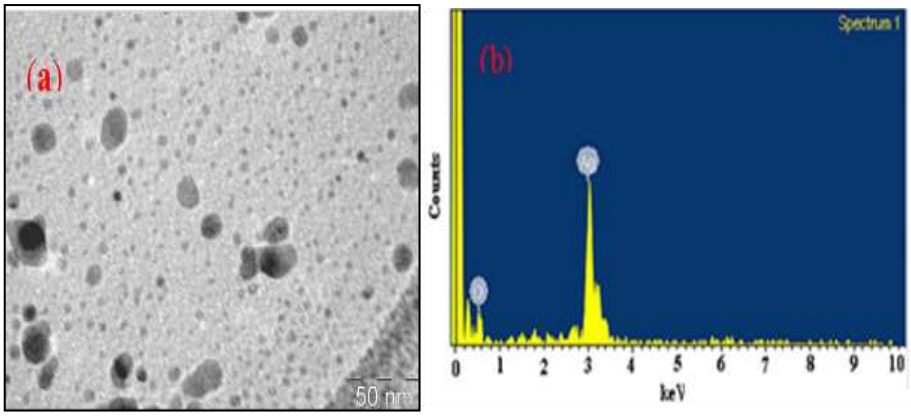

Figure 2.3 a) TEM image b) EDS images of AgPS

2.2.4 FT-IR spectroscopy

In order to identify the capping agents and the molecules responsible for the reduction of silver ions in palm shell extract, FTIR measurements of the palm shell extract was also carried out. Figure 2.4 shows the FT-IR spectrum of palm shell extract and silver nanoparticles. Table 2.2 shows the stretching frequencies of PS and AgPS. The bands appearing in the FTIR spectrum of the extract between 1000 cm^{-1} and 1260 cm^{-1} can be attributed to C–O vibrations of carboxylic acids, alcohols and phenols; and C–N vibrations of amines and amides. The peak at 1383 cm^{-1} can be attributed to aliphatic CH_2 and CH_3 groups, CH_2 groups of aldehydes and ketones, bending modes of O–H bonds in alcohols and phenols and carboxylic acids.

The FTIR spectrum recorded for the dried AgPS revealed bands at 1632 cm^{-1} and 1567cm^{-1} corresponding to the amide I and II bands of proteins respectively released from the palm shell [66]. The band at 2921 cm^{-1} can be assigned to the stretching vibrations of secondary amines. However, the stretching vibration of primary amines was not observed. The band at 1029 cm^{-1} of silver nanoparticles corresponds to the C–N stretching vibration of aliphatic amines or to alcohols/ phenols. The bands at 1762cm^{-1} and 2921 cm^{-1} can be assigned to the carbonyl groups and secondary amines, respectively. The bands between 400 cm^{-1} and 800 cm^{-1} in the IR spectrum of the extract can be attributed to bending vibrations from C-H bond of acetylenic groups, deformation and rocking modes of aliphatic CH_3, NH_2 groups, N–H wagging modes of amines as well as olefinic cis-CH= CH, and the out-of plane bending vibrations of the alcoholic and phenolic O–Hbonds [71].

This indicates that the synthesized silver nanoparticles are encapsulated by polysaccharides, proteins and phenols having functional groups of amines, alcohols, ketones, aldehydes, and carboxylic acids resulting in the stability of the nanoparticles [72, 73].There are earlier reports suggesting NADH- dependent reductases [42, 48], polyphenols and polysaccharides [49] as factors involved in reduction and stabilization of the nanoparticles. The coastal plants are generally reported to be rich in polyphenolic compounds [50]. In palm shell extract, the reduction process of metal ions could not have occurred by enzymes as the extract has been heated up to 80 ^{0}C. The carbonyl, phenolic and carboxyl groups could therefore be responsible for the reductive formation and stabilization of nanoparticles.

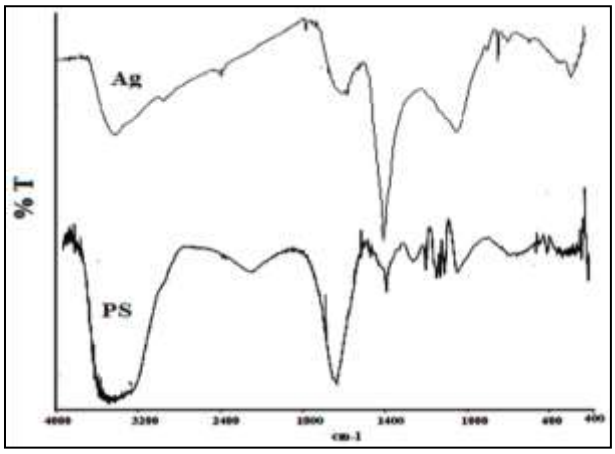

Figure 2.4 FT-IR spectrum of palm shell extract and silver nanoparticles

Table 2.2 IR Stretching frequencies of PS and AgPS

PS	**AgPS**	**Inference**
3400	3402	-OH stretching vibration
2078	2921,2364	–C-H stretching vibration of the –CH_2 group
	1762,1717	carbonyl group stretching
1632	1561	amide 1° and amide 2° bands of Chitosan matrix
1284,1192,1104	1029	C–C stretching vibration and asymmetric C–H bending of CH2 group
1383		stretching of aliphatic CH_2 and CH_3 groups
	876,825	C-H in plane bending mode/ out of plane deformation
714	774	Skeletal mode of vibration of anomeric carbons
638,601	529	metal-oxygen bond

2.2.5 X-Ray diffraction studies

The XRD pattern of the palm shell extract stabilized silver nanoparticles is shown in Figure 2.5. The synthesized silver nanoparticles correspond to face centered cubic phase of metallic silver. The diffraction peaks present in the spectra at 2θ values 38.89°, 43.24°, 64.69° and 78.04° can be assigned to the (111), (200), (220) and (311) reflections of the fcc structure of metallic silver. Analysis of the Bragg's peaks was undertaken to calculate the crystallite size using the Scherrer formula, $D=k\lambda/\beta\cos\theta$ where D is the crystallite size, k is a constant (=0.9 assuming that the particles are spherical), λ is the wavelength of the X-ray radiation which is 15.74nm, β is the line width (obtained after correction for the instrumental broadening) and θ is the angle of diffraction. The average particle size obtained from XRD data was found to be about 77.61nm

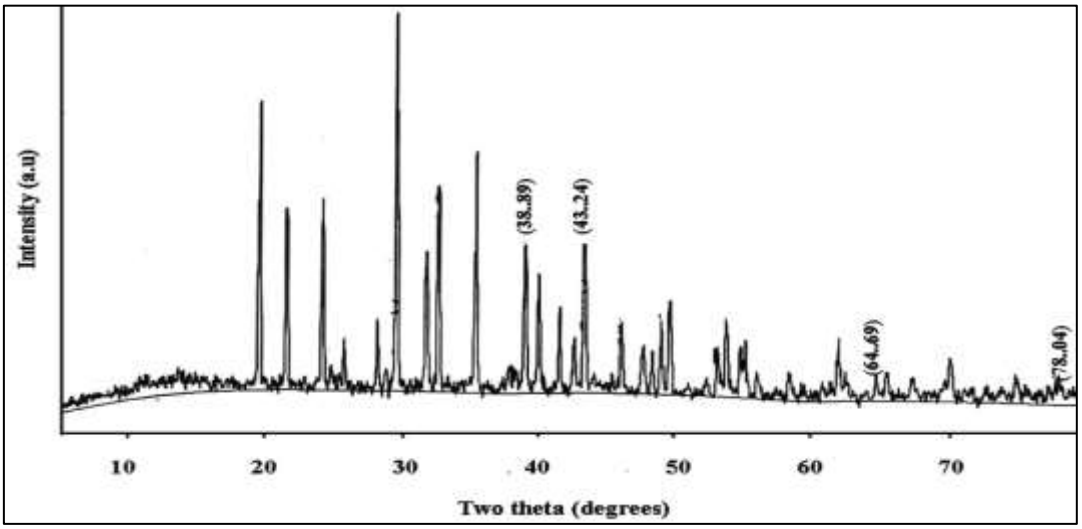

Figure 2.5 x-ray diffraction patterns of AgPS

2.2.6 Raman spectroscopy studies

Figure 2.6 shows the Raman spectra of AgPS. The peaks at 1351 cm^{-1} and 1594 cm^{-1} can be assigned to symmetrical and asymmetrical C=O stretching vibrations respectively while the peak at 1607 cm^{-1} can be attributed to aromatic C-H stretching in AgPS. Further the peak at 1045 cm^{-1} can be assigned to C–H in plane bending of the saccharides present in extract while the peaks at 835cm^{-1} and 1045 cm^{-1} can be attributed to skeletal vibrations associated with the β linkages, and C–C as well as C–O stretching, respectively [101].

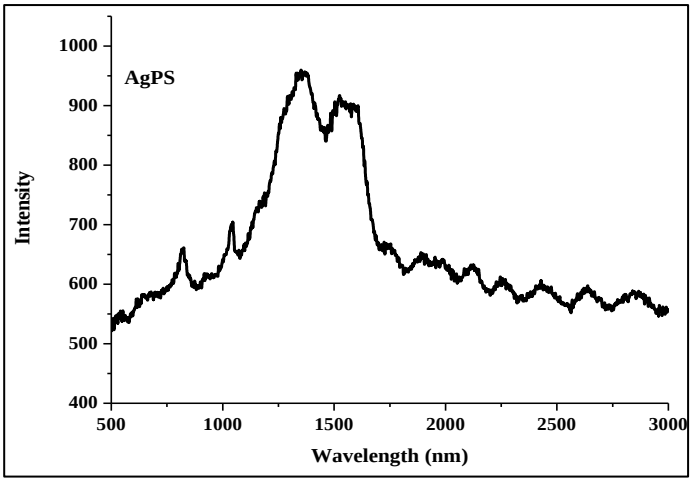

Figure 2.6 Raman spectra of AgPS

The SERS activity of AgPS was examined using RB-21, RR-141 and Rh6G as probe molecules. The Raman spectra of RB-21 and RB-21 adsorbed onto silver nanoparticles (AgPS-RB) are shown in Figure 2.7. The spectra of RB-21 are dominated by strong in-plane stretching and breathing modes of the phthalocyanine macrocycle. The bands observed are assigned based on the reported literature. The peaks observed for RB-21 at 613 $cm^{-1}$and 647 $cm^{-1}$are assigned to out of plane C-H bending. The band for macrocycle deformation at 746 cm^{-1} for RB-21 has been shifted to 717cm^{-1} in AgPS-RB. The peak at 1246 cm^{-1} may be due to pyrrole breathing. The peak at 1495cm^{-1} and 1573 cm^{-1} can be attributed to isoindole and C=C stretching frequency. The benzene ring stretching frequency of RB-21at 1598 cm^{-1}has been enhanced after loading RB-21 onto AgPS. Similarly, the C=N stretching at 1750cm^{-1} is enhanced 12 times after loading of RB-21 onto AgPS.

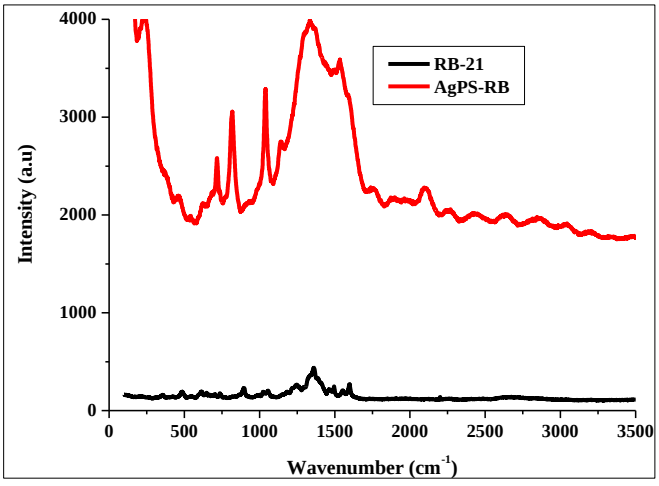

Figure 2.7 Raman spectra of RB-21 and AgPS-RB

Figure 2.8 shows the Raman spectra of RR141 and the RR141 adsorbed onto silver nanoparticles (AgPS-RR). The peak at 1651 cm^{-1} for RR-141 is attributed to ring vibrations and C=O stretching. The peak at 1384 cm^{-1} is indicative of N=N stretching. The peaks at 1008 cm^{-1}, 1320 cm^{-1} and 1146 cm^{-1} were attributed to C-S stretching, N=N stretching and C-N stretching vibrations. After adsorption of the dye onto AgPS (AgPS-RR) the C-S stretching frequency has been shifted to 1045 $cm^{-1}$with enhancement in intensity. The peak at 1585 cm^{-1} might be due to the aromatic ring chain vibrations. The medium intensity peak at 1241 cm^{-1}could be assigned to C=N stretching.

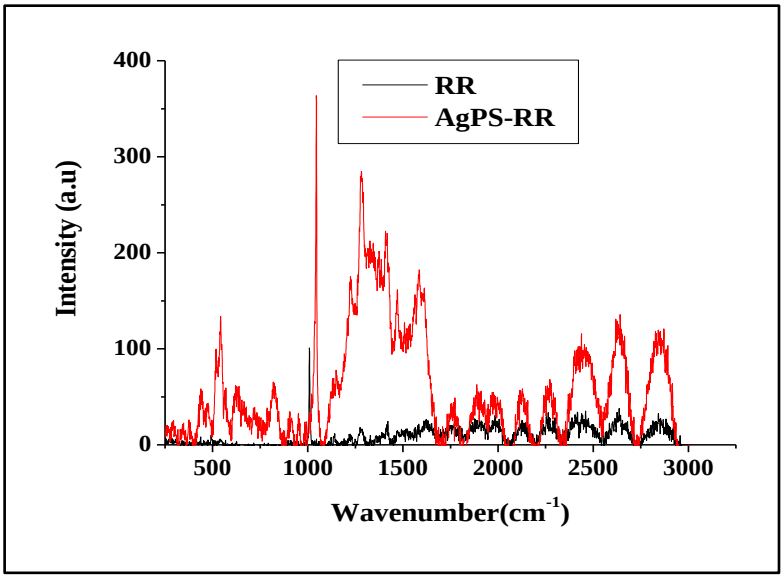

Figure 2.8 Raman spectra of RR-141 and AgPS-RR

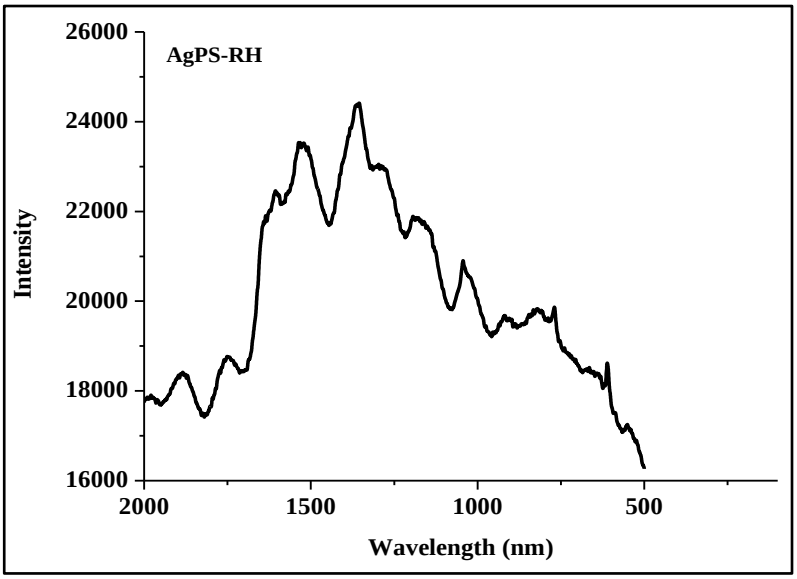

Figure 2.9 Raman spectra of AgPS-Rh

The Raman spectra of Rh-6G adsorbed onto Silver nanoparticles (AgPS-Rh) is shown in Figure 2.9. Raman spectrum for rhodamine 6G by excitation at 535nm was featureless which could be due to the strong fluorescence background at this wavelength and hence could not be shown in figure [74]. However, the SERS spectrum of Rh6G adsorbed on prepared Ag NPs was observed to be well defined. The bands at 1650 $cm^{-1}$and 1361cm^{-1}, can be assigned to C- C stretching modes, 1026cm^{-1}, 770cm^{-1} to C-H out-of-plane bending mode, and 658cm^{-1} to C- C- C ring in-plane vibration modes. The bands at 1306cm^{-1} and 1506 cm^{-1} can be attributed to N-H in-plane bending modes while the bands at 1181 cm^{-1} can be assigned to C-H in-plane bending modes. All the assigned bands are consistent with literature data on the Raman transitions of the Rhodamine 6G molecule. The SERS intensities of the signals for Rh6G observed on AgPS were ~2.4 x10^4 times enhanced. This increase in intensity is significant in comparison with the reported SERS spectra recorded on various other metal nanoparticles [75, 76].

For the first time Ag nanoparticle aggregates formed by reduction using Palm shell extract has been studied as SERS substrates. The process did not require deposition on any substrate and the capping was suitable to produce hotspots for sufficient SERS [78]. The average size of AgPS was 55 nm which was optimum for SERS enhancement as reported in literature [79]. AgPS could function as SERS substrates due to extremely strong local electromagnetic field enhancement from hotspots which could probably be present in anisotropic AgPS [80-82]. The negative zeta potential of the nanoparticles is further suited to give an enhanced SERS detection through short-range interactions between the Rh6G molecules and AgPS [75].

2.2.7 Degradation of individual dyes (Reactive blue-21, Reactive red -141, Rhodamine 6G) and mixture of the dyes (RB+RH, RB+RR, and RR+RH)

The potential of AgPS in the presence of H_2O_2 for catalytic oxidation of reactive blue 21, Reactive red 141, Rhodamine 6G as well as binary mixture of dyes was investigated. Figure 2.10 shows the UV spectra for degradation of RB-21, RR-141 and Rh-6G using silver nanoparticles and H_2O_2. It clearly indicates that it took 6 h and 3.5 h for complete degradation of 100 ppm RB-21and RR-141 respectively in the presence of AgPS and H_2O_2. It was observed that complete degradation of Rhodamine 6G in the presence of catalyst and $H_2O_2$was not achieved even after 24 hrs. Figure 2.11 shows the UV spectra for mixture of dyes wherein both the dyes were taken at equal concentration and equal volume (100ppm and 5 mL). It was observed that in the case of RB+RH after 10 h 65% degradation had occurred while complete

degradation required 24h. It was observed that 80% of RB+RR and 66% of RR+RH degraded after 24h interval. It is felt that reactive blue containing copper phthalocyanine could also be playing a catalytic role in the degradation of Rh6G [77] as complete degradation of RR+ RH did not occur even after 24h, Rh6G as a single component could not be degraded in 24h while complete degradation of RB + RH occurred in 24h. This could be due to xanthenes ring structure of Rh6G which cannot be degraded with ease. Degradation of the dyes did not occur in the presence of only30% H_2O_2, indicating there was no direct oxidation pathway by peroxide. However, degradation occurred in the presence of 30% $H_2O_2$and the nanoparticles, suggesting that degradation could be via free radical pathways.

After each experiment, the catalyst was carefully separated from the solution, washed with water and further used in the next cycle. The above catalytic process was repeated for 4 cycles for individual and mixture of dyes. After 3 cycles (fig 2.12) of catalytic process it was that observed that efficiency decreased by 2-3% and this indicates efficient reusability of the catalyst.

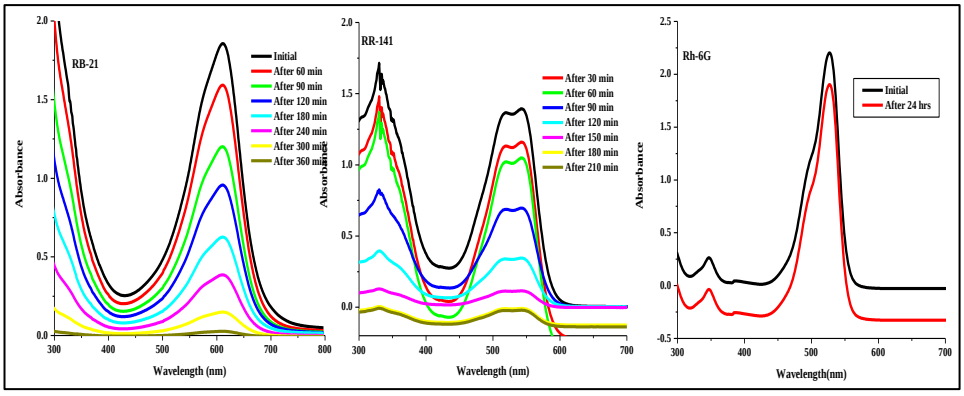

pH 6; RT; Concentration 100 ppm, 3 mL; 0.5 mg catalyst; 200 µL H_2O_2

Figure 2.10 UV spectra for degradation of RB- 21, RR-141 and Rg-6G using silver nanoparticles and H_2O_2

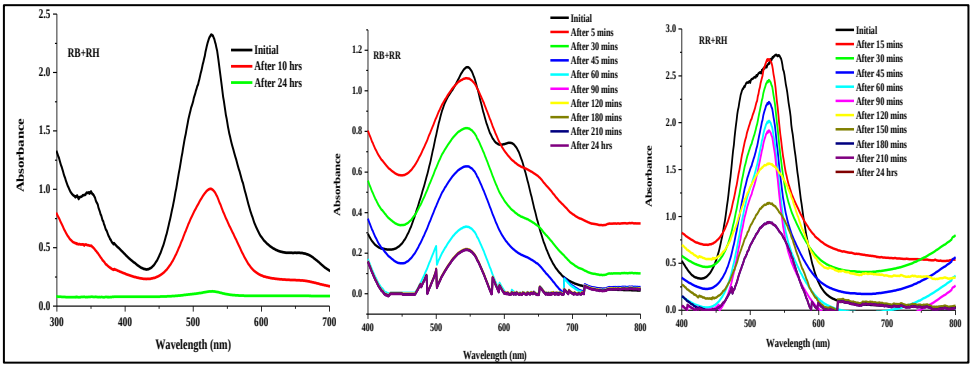

pH 6; RT; Concentration 100 ppm, 3 ml; 0.5 mg catalyst; 200 µL H_2O_2

Figure 2.11 UVspectra for mixture of dyes in the presence of AgPSand H_2O_2.

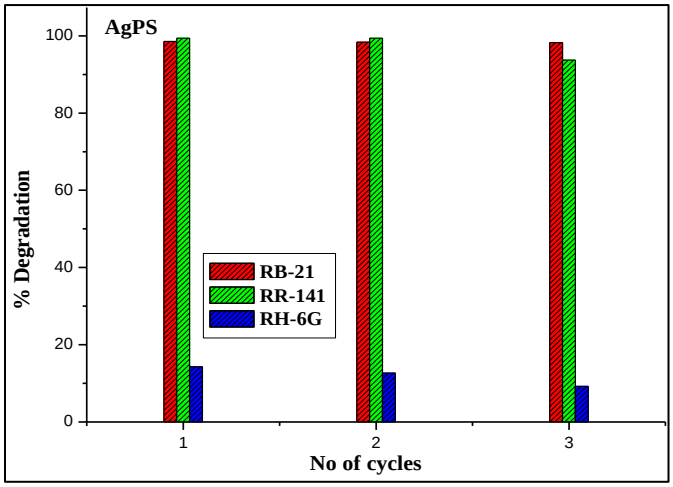

Figure 2.12 Catalyst reusability studies of RB-21, RR-141 and Rh-6G using AgPS

2.2.8 Total organic content

The mineralization of organic carbon of the dyes in single component systems or in binary components was investigated by Total Organic Carbon (TOC) measurements; has been represented in Figure 2.13. It was observed that there was 47, 30 and 74% reduction in TOC for RB-21, RR-141 and Rh-6G respectively in single component dye systems and. 29, 32 and 59% for RB+RH, RR+RH and RB+RR binary systems respectively. The TOC reduction is lesser than decolorization which may be due to the formation of smaller uncolored products.

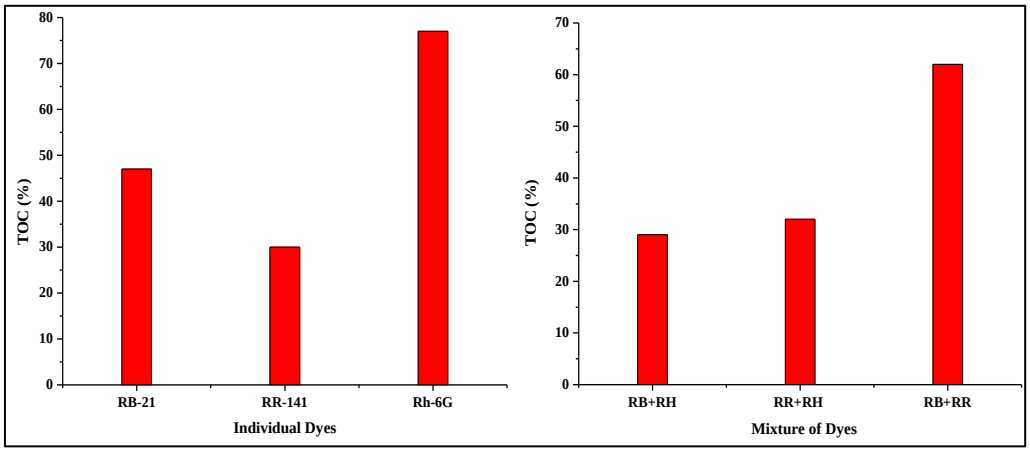

Figure 2.13 Total organic content of degraded dyes

2.2.9 Catalytic reduction of p-nitrophenol

The catalytic properties of AgPS were further examined by investigating the reduction of toxic pollutant p-nitrophenol in the presence of $NaBH_4$which is a widely used model used model reaction to study the catalytic potential of nanoparticles . The

absorption spectra of the reduction of 4-nitrophenol catalyzed by AgPSis shown in Figure 2.14. The reduction reaction of 4-nitrophenol was initiated, as soon as the catalyst was added into 4-nitrophenol. It was observed that the intensity of 401 nm band of p-nitrophenol decreased, with the simultaneous appearance of a new band at 298 nm, corresponding to the formation of 4-aminophenol in the solution.

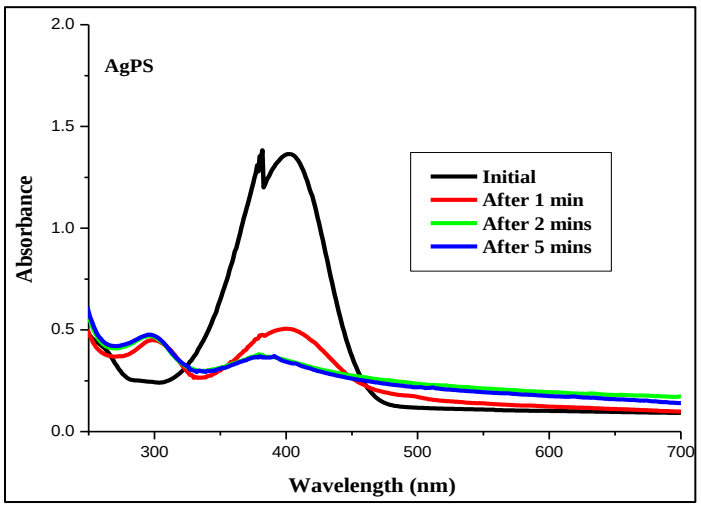

Figure 2.14 Reduction of 4-nitrophenol using AgPS

2.2.10 Conclusion

The present study reports the facile biogenic synthesis of silver nanoparticles from silver nitrate using palm shell extract. The method adopted is green as the palm shell extract serves as both reducing and stabilizing agent for the silver nanoparticles synthesized. The abundance of hydroxyl and carboxyl groups facilitates the complexation of silver ions and could probably be subsequently, reduced to elemental silver by in situ oxidation of hydroxyl groups; and by the intrinsic carbonyl groups of aldehydes. This proposed mechanism is substantiated by the FTIR and Raman spectroscopic data. Notably, enhancement of Raman bands of the organic capping agents bound to the silver colloids facilitates these nanoparticles as suitable substrates for SERS.

The work may provide a potential application of Ag nanostructure materials in the field of SERS a as well as catalysts for degradation of environmental contaminants.

Guargum Stabilized Silver nanoparticles - SERS substrate for dye detection and as catalyst for degradation of cationic and anionic dyes

2.3. Introduction

In addition to plant extracts gums and polymers have been used for stabilizing colloidal metal dispersions. For instance, gums such as gum Acacia [71] and gum kondagogu [86,87] microbial polysaccharides, gum gellan [88] and carboxymethylated-curdlan and marine polysaccharide gums including fucoidan [89] and alginate [90] have been investigated as reducing and stabilizing agents for silver, gold and platinum nanoparticle biosynthesis. They are gaining interest as matrix materials for immobilization of nanoparticles due to their ability to act as reducing agents, control particle growth as well as stabilize the particles, thus resulting in biogenic nano materials with new or improved properties [91]. In this category, guargum (GG) is a well-known polysaccharide with a high molecular weight, isolated from the seeds of leguminous herbs [92]. It consists of long linear β-(1-4) mannose backbone units to which α-(1-6) galactopyranoside single subunits are attached as side chains [93].GG is a non-ionic polydisperse rod-shaped polymer consisting of about 10,000 residues. E S Abdel Halim et al reported the use of polyacrylamide/guar gum graft copolymer for preparation of silver nanoparticles [94]. They observed that silver nanoparticles could be formed using GG at pH 12.5 by heating to 70^0C. However, they had observed that polyacrylamide/guar gum was more advantageous because the structure and properties of the biopolymer could be modified after grafting and could function as a better stabilizing agent.

In the present work we have attempted to use Guargum (G) as reducing and stabilizing agent under ambient conditions for green synthesis of silver nanoparticles (GAg) and explored its potential applications as SERS substrate as well as catalyst for the degradation of single and binary mixture of dyes. Rhodamine 6G (Rh6G), Reactive blue-21 (RB-21) and Reactive red-141 (RR-141) were used as probe molecules for SERS detection and as model dyes for degradation studies.

2.3.1 Materials and methods

Silver nitrate (Merck, 99.9%), 4-nitrophenol (extrapure AR) Guargum (SRL, 95%).Commercially used dyes Reactive blue-21(RB-21), Reactive red-141, Rhodamine-6G (RH-6G), hydrogen peroxide (H_2O_2, Fisher Scientific; 30%solution), were used in this study without further purification.

2.3.2 Synthesis of Guargum stabilized silver nanoparticles

A solution of 0.1M $AgNO_3$was added to 0.5 % aqueous guargum(G) solution. The pH of the solution was raised to 10 by dropwise addition of 0.1 N NaOH. The solution was stirred with a glass rod for 1 min and allowed to stand at room temperature for 5min.Formation of black silver nanoparticles (GAg) was observed. Characterization studies of GAg were done as mentioned in section 2.1.3

2.4 Results and discussions

2.4.1 Zeta potential analysis

Fig 2.15 shows the zeta potential curve for the synthesized nanoparticles in the pH range 1- 11. The zeta potential of GAg was found to be negative in the pH range studied with a value of -52.61 mV at pH 9 and -47 mv at pH 7 respectively contributing to the stability of the nanoparticles.

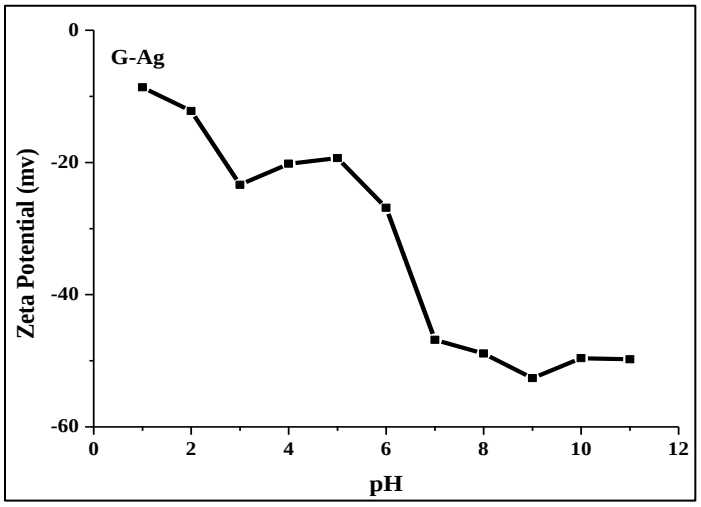

Figure 2.15 Zeta potential curve for the synthesized silver nanoparticles

2.4.2 UV-Vis Absorption Spectroscopy

The UV-vis spectrum of silver nanoparticles (GAg) is shown in Figure 2.1.6.A broad intense surface plasmon resonance (SPR) peak at 446 nm was observed. A time resolved spectra could not be shown as the nanoparticles formed in a short span of 5 min. The nanoparticle formation was found to take place at alkaline pH (pH 9 and above). There was no difference in

the nature of GAg formed in the pH range 9 and above. It was decided to maintain the pH at 9, so as to avoid large additions of NaOH in our endeavour to maintain the process as green as possible. There were no peaks observed at ~335 and 560 nm, indicating the complete absence of nanoparticle aggregation [68, 71]

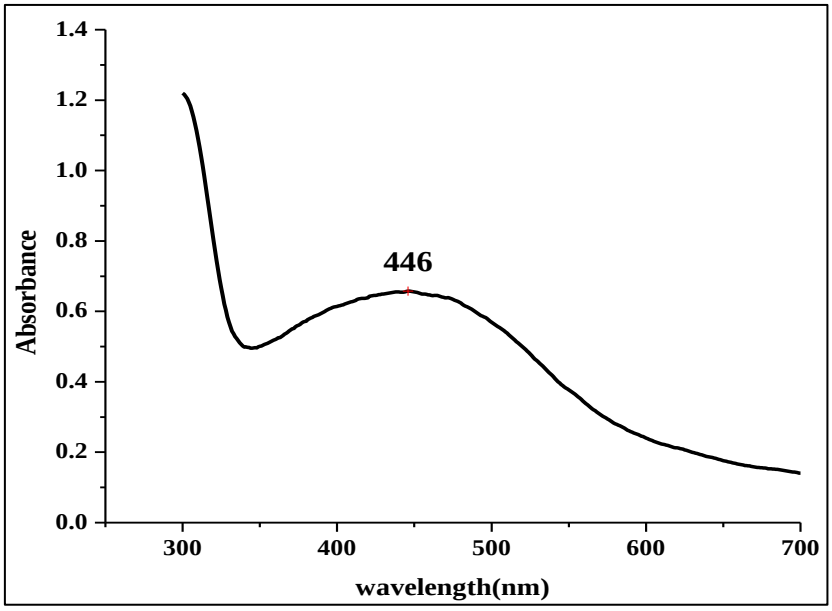

Optimum parameters pH=9, RT, 0.1 N $AgNO_3$ solution

Figure 2.16UV –Vis spectra of silver nanoparticles synthesized using Guargum

2.4.3 Morphology of Guargum stabilized nanosilver

Figure 2.17 shows the TEM images and EDAX spectrum of silver nanoparticles. The figure shows that the formed Ag nanoparticles were uniformly spherical and were embedded in the guargum matrix as a cluster with an average diameter of about 50 nm. The EDAX spectrum of silver nanoparticles confirmed the presence of silver in guargum matrix. These nanoparticles were observed to be stable in aqueous solution over a period of 30 days.

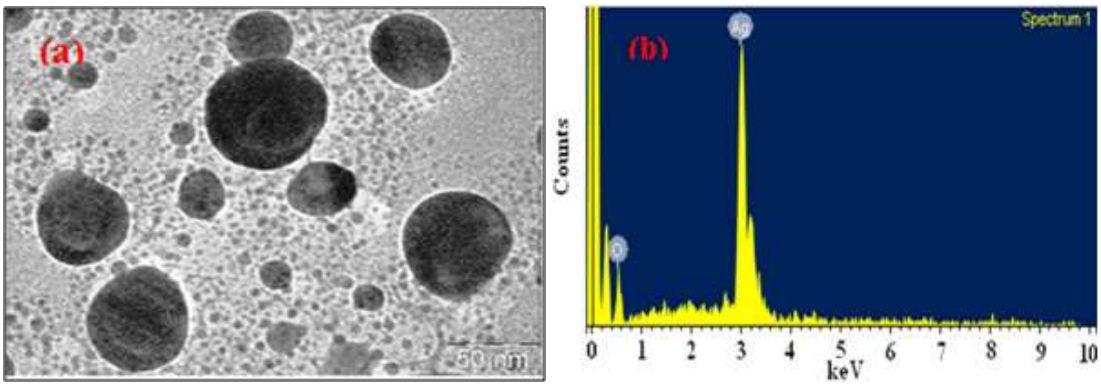

Figure 2.17 shows the a) TEM image b) EDS images of GAg

2.4.4 FT-IR spectroscopy

Figure 2.18 shows the FT-IR spectrum of G and GAg. Table 2.3 shows the IR stretching frequencies and their assignments for G and GAg. The peaks at 3417 cm^{-1} and 3487 cm^{-1} for G and GAg are indicative of the presence of OH group. Furthermore it is observed that OH of GAg is broader in comparison with G which can be attributed to the interaction of the silver nanoparticles with the hydroxyl groups of guargum. The bands at 2189, 1469 and 1249 cm^{-1} for G and the bands at 2085, 1485 and 1222 cm^{-1} for Gag correspond to asymmetric stretching, scissoring; as well as twisting and rocking vibrations of methylene groups, respectively. A shift of frequencies is observed in the spectrum of GAg as compared to G which clearly indicates the capping of the guargum onto the silver nanoparticles. The peaks at 1641 and 1654cm^{-1} in the spectra of G and GAg respectively correspond to the asymmetrical stretch of carboxylate groups which could be attributed to the involvement of the carboxylate group in the capping of Ag nanoparticles. The peaks at 1469 and 1485cm^{-1} are indicative of -C-H bending vibrations while the peaks at 1058 and 1055 cm^{-1} can be attributed to-OH bending vibrations for G and GAg respectively [84].

Table 2.3 IR stretching frequencies of G and GAg

G	**GAg**	**Inference**
3646,3417, 3241,3062	3487,3247,3072	-OH stretching
2351,2181	2360,2175,2080	asymmetric stretching, scissoring; as well as twisting and rocking vibrations of methylene groups
1651,1644	1692,1654	asymmetrical stretch of carboxylate group
1469	1480,1465	-C-H bending vibrations
1249,1178,1058	1222,1178,1055	-OH bending vibrations
870	930	skeleton mode of the anomeric skeletal configuration and glycosidic linkages

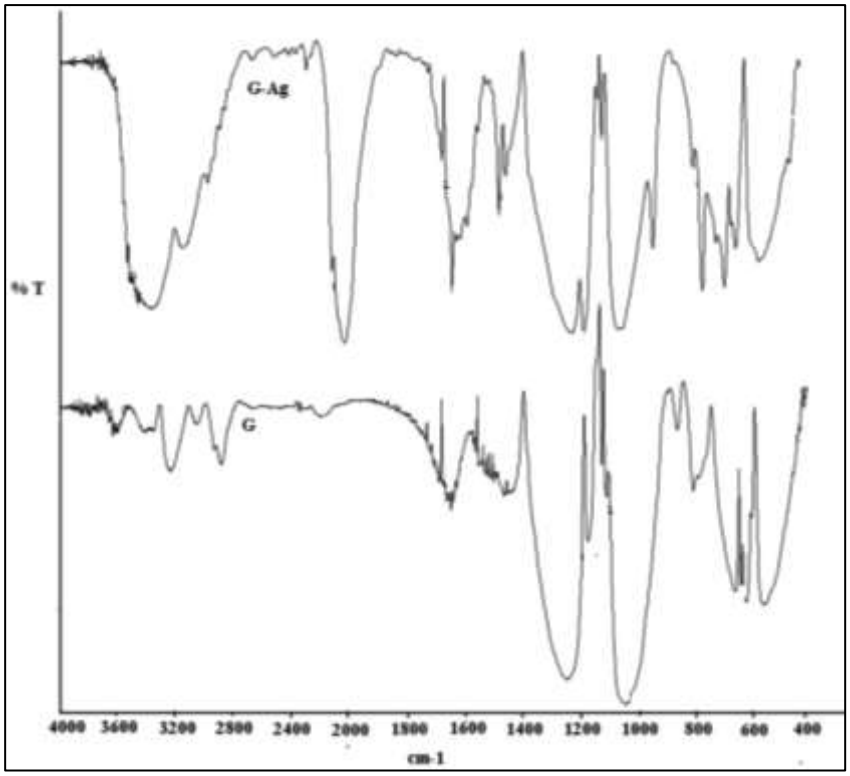

Figure 2.18 IRspectrum of Guargum and the silver nanoparticles synthesized using Guargum

2.4.5 X-Ray diffraction studies

The XRD pattern of GAg is shown in Fig 2.19, which corresponds to fcc phase of metallic silver. The diffraction peaks present in the spectra at 2θ values 38.52^0, 44.75^0, 64.990 and 77.87^0 could be indexed to the (111), (200), (220) and (311) reflections of the fcc structure of metallic silver. Analysis of the Bragg's peaks was undertaken to calculate the crystallite size using the Scherrer formula, as mentioned in section 2.13. The average particle size obtained from XRD data is found to be about 49nm [95].

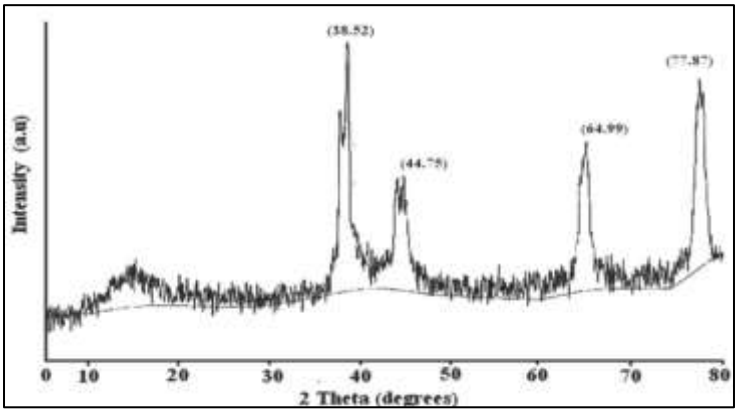

Figure 2.19 XRD spectrum of the silver nanoparticles synthesized using Guargum

2.4.6 Raman spectroscopy studies

Figure 2.20 shows the Raman spectra of GAg. The spectrum showed a strong and sharp band at 298 cm^{-1}, which could be attributed to Ag–O bonds [96]. This peak indicated the formation of a chemical bond between silver and carboxylate groups of Guargum molecules suggesting that guar gum is bound to the silver surface through carboxylate groups. This Ag–O bond probably resulted in SERS band broadening [97]. The bands at 1322 cm^{-1} and 1537 cm^{-1} correspond to symmetric and asymmetric C= O stretching vibrations of carboxylate group. Further, the peak at 1054 cm^{-1} could be assigned to C–H in plane bending of the saccharides present in guargum. These vibrations clearly indicate that guargum is involved in capping and stabilizing of the silver nanoparticles.

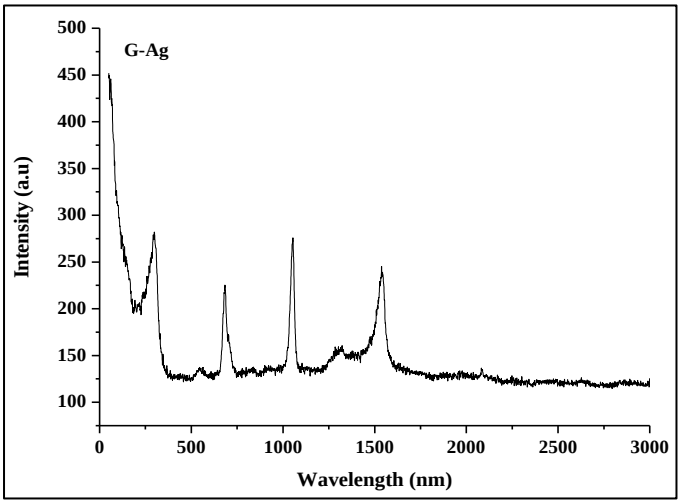

Figure 2.20 Raman spectra of Guargumstabilized Silver Nanoparticles (GAg)

Figure 2.21 shows the Raman spectra of RB-21and RB-21 deposited on GAg (GAg-RB). The spectrum of RB-21 shows strong in-plane stretching and breathing modes of the phthalocyanine macrocycle. The peak at 1598 cm^{-1} can be attributed to ring C-C stretching. The peak observed at 613$cm^{-1}$for GAg-RB can be assigned to out of plane C-H bending while the peak at ~642cm^{-1} in RB and GAg-RB can be ascribed to ring breathing. The peak at 238 cm^{-1} is assigned to Ag-O stretching in GAg which has been slightly shifted after loading RB-21to298 cm^{-1}[98]. The band at ~897 cm^{-1} in RB and GAg-RB can be attributed to ring skeletal vibration while the peak at ~1362cm^{-1} can be attributed to C-C/C-N stretching. No significant amplification was observed in the Raman spectra of GAg-RB.

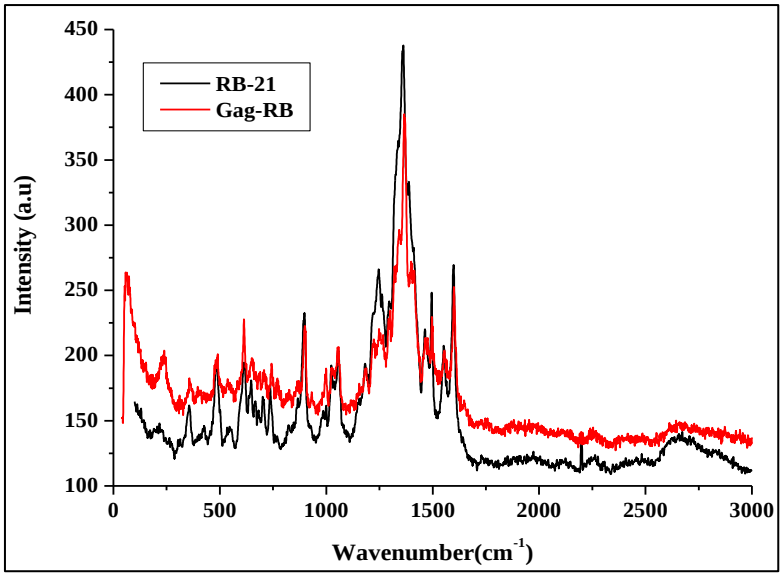

Figure 2.21 Raman spectra of RB-21 and GAg-RB

Figure 2.22 shows the Raman spectra of RR-141and RR-141 deposited on GAg (GAg-RR). The peak at 1651 $cm^{-1}$for RR-141canbe attributed to a combination of ring vibrations and C=O stretching. The peaks at 1008 $cm^{-1}$and 1285 cm^{-1} are attributed to C-C stretching and N=N stretching vibrations respectively. The band at 2880 cm^{-1} can be attributed to C-H stretching. After adsorption of RR-141 the C-C stretching frequency at 1008 cm^{-1} has disappeared and the peak at 1651 for C=O stretching has been shifted to 1674 cm^{-1} with an enhancement in intensity indicating the interaction of the dye with nanoparticles. The band at ~1580cm^{-1} and ~1281cm^{-1} for RR-141 and GAg-RR141 can be attributed to C-N stretching and C=O bending vibration respectively while the Cu-N band is observed at ~377cm^{-1}.

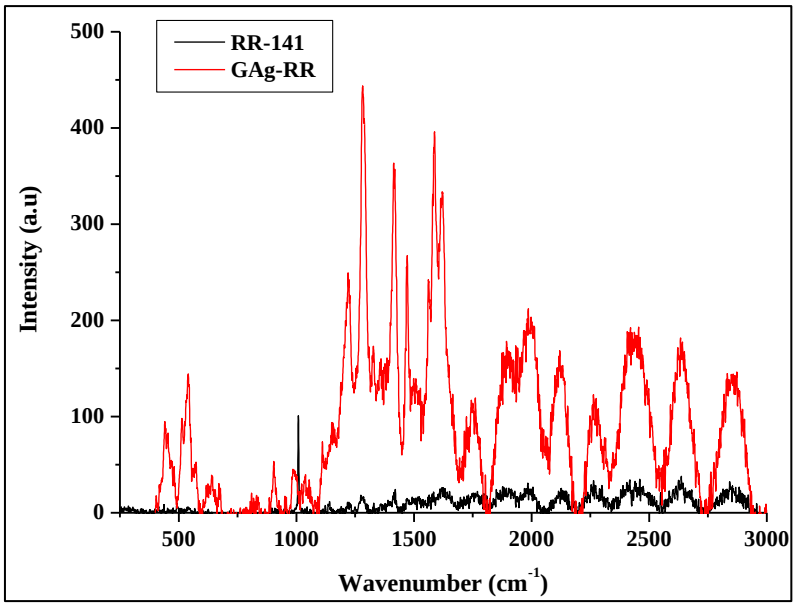

Figure 2.22 Raman spectra of RR-141 and GAg-RR

Figure 2.23 shows the Raman spectra of Rh-6G loaded silver nanoparticles (GAg-RH). The bands at 610,770 and 1182 cm^{-1}can be assigned to C–C–C ring in-plane bending, out-of-plane bending motion of the hydrogen atoms of the xanthene skeleton and C–H stretching vibrations, respectively, while the bands at 1360, 1506 and 1647 cm^{-1} are attributed to the aromatic C–C stretching vibrations of Rh6G molecules [87] The band at 1388cm^{-1} for Rh-6G can be attributed to N–phenyl stretching and the band at 1599cm^{-1} can be assigned to aromatic C-C stretching. The band at ~1509 cm^{-1} and ~ 1362 $cm^{-1}$for GAg-RH can be attributed to aromatic C-C stretching and C-N stretching respectively where the intensity of the signals has been enhanced on an average 2.5 X 10^4 times after loading of dyes.

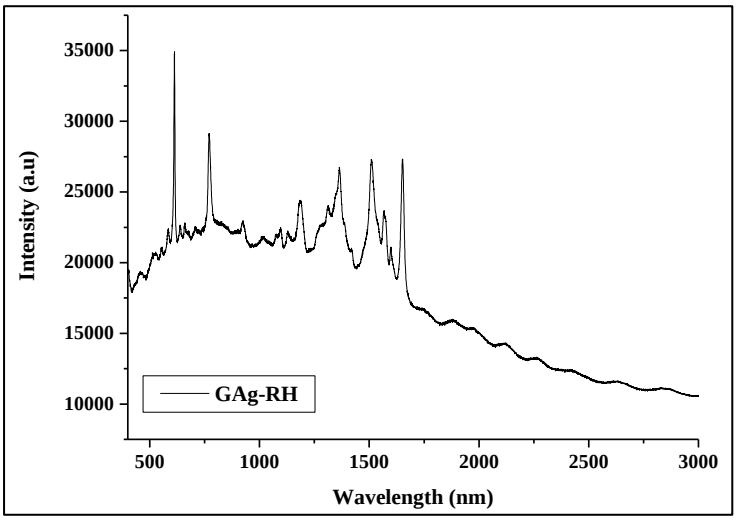

Figure 2.23 Raman spectra of GAg-RH

The SERS intensities of the signals for GAg-RH, GAg–RR and GAg–RB were greater than those observed for only Rh6G, RR141 and RB21 respectively. This increase in intensity for Rh6G was significant (10^4 times) in comparison with the reported SERS spectra in literature. The strong surface enhancement for the Raman spectra of Rh 6G could be due to several factors i.e., enhancement of electromagnetic field, adsorption of the dye molecule (molecular resonance enhancement) as well as an additional enhancement due to a specific interaction between the molecule and GAg (chemical enhancement) [74]. However, the SERS enhancement was found to be only 3 times in the case of RB21 and RR 141 which could probably be due to their being anionic dyes. Enhancement of the Raman signal for the cationic form of Rh6G could also be of electromagnetic nature due to Coulomb interactions between the positively charged xanthene part of rhodamine and the negatively charged silver surface.

2.4.7 Mechanism for the formation of Silver nanoparticles

Earlier characterization studies revealed the presence of abundant hydroxyl, carbonyl and carboxylic functional groups in Guargum. The presence of negatively charged groups could be also confirmed from the negative zeta potential value of -52.61V. The large number of hydroxyl and carboxylic groups on GG facilitates the complexation of silver ions which further could oxidize the hydroxyl groups to carbonyl groups and in the process got reduced to elemental silver. Further, these nanoparticles were also capped and stabilized by the polysaccharides along with the proteins present in guargum [100]. A similar mechanism was reported by Vigneswaran et al where soluble starch, was used in synthesis of silver nanoparticles [101]. Mohan et al [86] produced silver nanoparticles using gum acacia, where the carboxylate groups were proposed to be involved in complexation of silver ions and were subsequently reduced by hydroxyl groups. Hydroxyl group mediated reduction was also reported for the synthesis of silver and gold nanoparticles with PEG [102], PVP [90] and alginate [103].

2.4.8 Degradation studies of individual and binary mixture of dyes

Figure 2.24 and Figure 2.25 shows the UV spectra for dye degradation of individual and binary mixture of dyes. The degradation studies were investigated with time using 200 μL of 30% hydrogen peroxide with GAg as a catalyst. The initial concentration of RB-21, RR-141, Rh-6G and binary mixture of dyes was 100 mg/L. Degradation of the dyes did not occur in the presence of only30% H_2O_2. However, complete degradation of RB- 21 occurred within 2 minutes by hand shaking in the presence of 30% H_2O_2 and GAg while complete degradation of RR-141 occurred after 30 min under stirred conditions using a magnetic stirrer. On the other hand complete degradation of Rh6G was observed after a time interval of 300 min. In binary mixtures, it was observed that 80% degradation occurred in the case of RB+RH in a time interval of 24 h while 91% degradation of RB+RR and 78% degradation of RR+RH were observed after 24 hrs. The recycling efficiency of the catalyst was tested. After each run, the catalyst was carefully separated from the solution, and then washed with water so that any possible remnants on the surface of the catalyst will be removed. The above catalytic process was repeated for 3 cycles for individual and mixture of dyes. After 3 cycle of catalytic process it was that observed that efficiency decreased by 2-3% and this indicates efficient reusability of the catalyst (Figure 2.26).

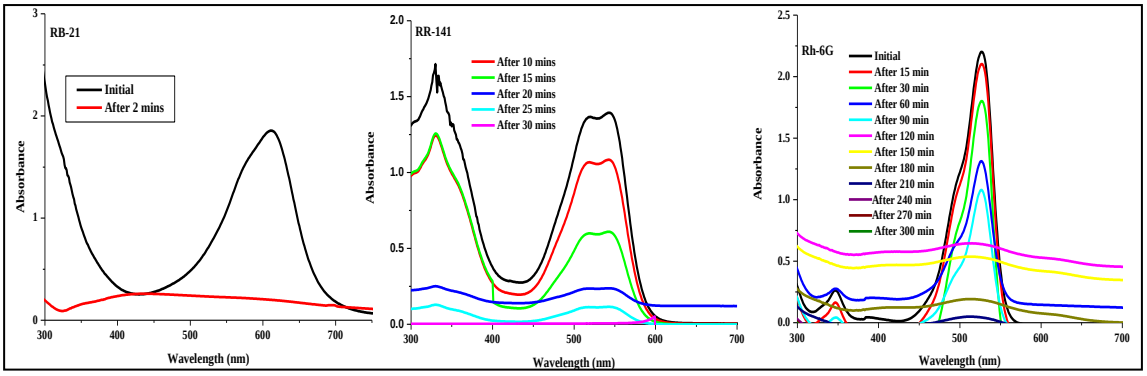

pH 6; RT; Concentration 100 ppm, 3 ml; 0.5 mg catalyst; 200 µL H_2O_2

Figure 2.24 Degradation of RB-21, RR-141 and Rh6Gin the presence of GAg and H_2O_2

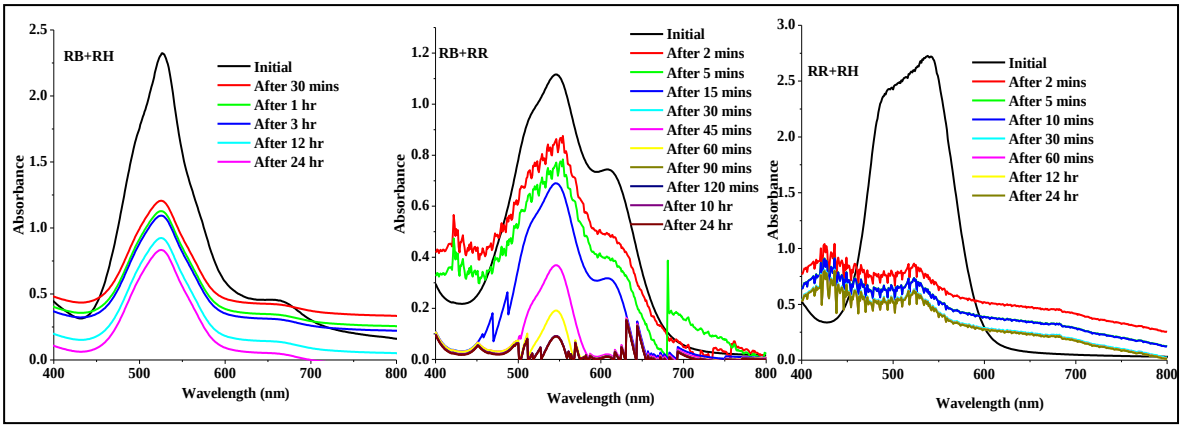

pH 6; RT; Concentration 100 ppm, 3 ml; 0.5 mg catalyst; 200 µL H_2O_2

Figure 2.25 Degradation of RB+RH, RB+RR and RR+RH in the presence of GAg and H_2O_2

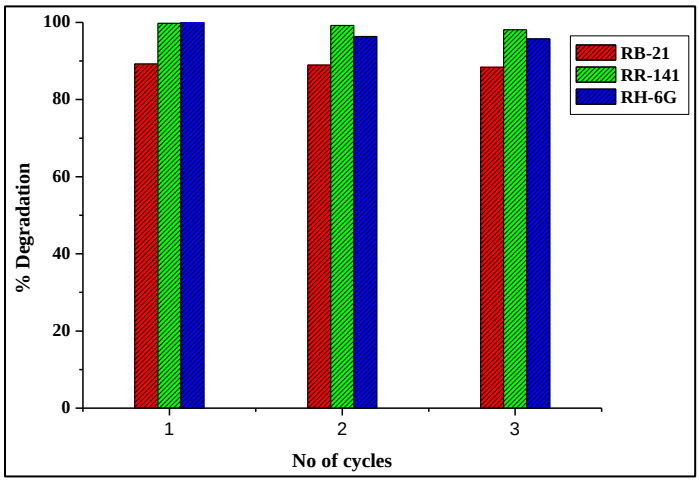

Figure 2.26 Reusability studies of GAg

2.4.9 Total organic content

The mineralization of organic carbon of the dyes in single component systems as well as in binary components was investigated by the Total Organic Carbon (TOC) (Figure 2.27). It was observed that there was 59, 41 and 77% reduction in TOC for RB-21, RR-141 and Rh6G respectively in single component system and 21, 37 and 62% reduction for RB+RH, RR+RH and RB+RR binary systems respectively. The TOC reduction is lesser than decolorization which may be due to the formation of smaller colourless products.

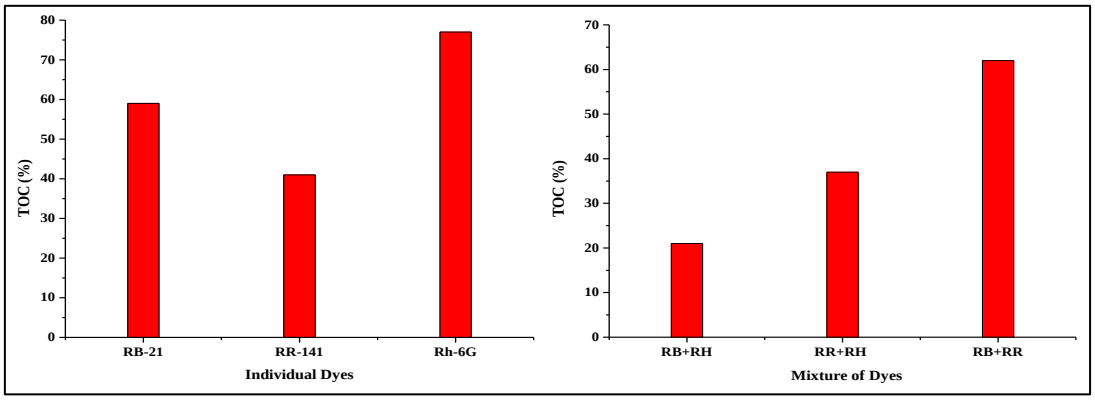

Figure 2.27 TOC reductions for individual and binary mixture of dyes

2.4.10 Catalytic reduction of p-nitrophenol

The catalytic properties of the Guargum stabilized silver nanoparticles were also examined for the reduction of toxic pollutant p-nitrophenol in the presence of sodium borohydride. Though the reduction of 4-NP to 4-AP using aqueous $NaBH_4$ is thermodynamically favorable, the presence of the kinetic barrier due to large potential difference between donor and acceptor molecules decreases the feasibility of this reaction. It is well-known that the metal NPs catalyze this reaction by facilitating electron relay from the donor BH_4^- to acceptor 4-NP to overcome the kinetic barrier. The conversion from 4-NP to 4-AP occurs via an intermediate 4-nitrophenolate ion formation. Figure 2.26 shows successive absorption spectra of 4-nitrophenolate ion at 401 nm. On addition of the Silver nanoparticles, there is a rapid decrease in the intensity of the absorption peak at 401 nm with the simultaneous appearance of a new band at 296 nm, corresponding to the formation of 4-aminophenol in the solution.

The absorption spectra of the reduction of 4-nitrophenol catalyzed by the silver nanoparticles are shown in Figure 2.27. It can be seen that the spectrum of the mixture of the 4-nitrophenol and borohydride solutions is dominated by the band at

401 nm, which corresponds to intermolecular charge transfer of 4-nitrophenol. The reduction reaction of 4-nitrophenol was initiated, as soon as silver nanoparticle was added into the mixture solution of reactants. It was observed that the intensity of 401 nm band of p-nitrophenol decreased, the catalyst was efficient upto 3 cycles.

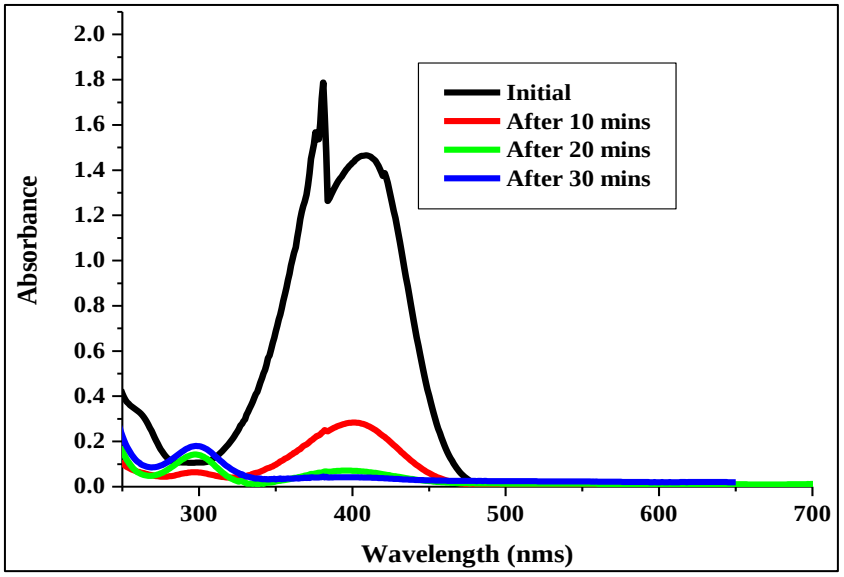

0.3 mg catalyst, 0.3 mL of 2 mM solution of 4-NP, and 1mL of 0.01M NaBH4

Figure 2.28 Reduction of p-nitrophenol using GAg as a catalyst

2.4.11 Conclusion

The synthesis of Silver nanoparticles using Guargum as a reducing and stabilizing agent was investigated. These nanoparticles were prepared at ambient temperature conditions. The synthesized silver nanoparticles effectively catalysed degradation of individual and binary mixture of cationic and anionic dyes during the process of degradation of H_2O_2.

Biosynthesis of Palm shell reduced Silver-Chitosan composite and Chitosan-Guargum silver composite for its environmental applications

2.5 Introduction

Encouraged with the effectiveness of Guargum as capping and reducing agent during the formation of silver nano and the catalytic efficiency of Guargum capped Ag nanoparticles in oxidative degradation of RB21, RR 141 and Rh6G as well as their effectiveness SERS substrates, it was felt that an attempt could be made to use chitosan as reducing and stabilising agent for the preparation of silver nano particles. An added advantage of using chitosan is its biocidal activity against bacteria, yeast, mould and simultaneous non-cytotoxic effects toward mammalian cells [108-111].

A brief survey of the literature revealed that chitosan, a biocompatible carbohydrate polymer, has been used as a reducing and stabilizing agent in a green synthesis of silver nanoparticles. A new strategy was reported comprising of an electrochemical technique was developed to prepare positively charged Ag ions, and a chemical method via aid of natural chitosan [112-115]. The SERS-active properties of the prepared Ag nanoparticles were also examined via probing Rh6G. However, these methods require heating at 95°C for prolonged intervals of around12 hrs. Our attempts to prepare chitosan capped silver nano also affirmed the fact that ambient conditions were not appropriate for the synthesis of chitosan capped silver nano. Furthermore, modification of chitosan through blending with other polymers and cross-linking are both convenient and effective in improving its physical properties for practical applications [116, 117]. There have been some reports [118-120] dealing with poly blends of chitosan with other natural or synthetic polymers. Recently, chitosan and poly (ethylene oxide) (PEO) blends have been reported for the preparation of membranes for haemodialysis [121,122]. Thus, the combined use of gum arabic with chitosan could provide an inter-biopolymer electrostatic complex that could form strong viscoelastic films around oil droplet sand provide them with good barrier properties against oxidation [123]. Lately, polymer blending has become a method of choice for obtaining polymeric materials with desirable properties for practical applications. Chitosan blended with poly (vinyl alcohol) (PVA) has been reported to have good mechanical and chemical properties [124-126]. The enhanced property has been attributed to the interactions between chitosan and PVA in the

blend through hydrophobic side chain aggregation and intermolecular and intramolecular hydrogen bonds [127]. However, the uncontrolled rate of hydration, decreased viscosity upon storage and microbial contamination limits its applications in the biomedical area. To improve its physicochemical properties, efforts have been made to develop the graft copolymer of Guar gum with other polymers like acrylamide for use in controlled release applications [128,124]. Chitosan–guargum(CG) composite has shown superior physico-chemical properties including tensile strength, hydrophilicity, antimicrobial properties, etc., and was reported to be also suitable for enzyme immobilisation [129, 130]. In this study, we used guargum–chitosan composite matrix for silver nanoparticle synthesis (CGAgPS). However, there are no reports on the use of blends as supports for nanoparticles. Preliminary investigations on the use of chitosan guargum blend in different ratios revealed that the blend was also not effective in reducing silver ions to silver nano. Since palm shell extract was efficient in reducing and capping agent during the formation of nano silver particles it was felt that the AgPS nanoparticles could be encapsulated in chitosan and chitosan guargum blend. Heterogeneous catalysis by chitosan-AgNPs composite was reported for the reduction of 4-NP to 4-AP [131, 132].

In the present investigation a Chitosan-silver nanocomposite (CAgPS) and a Chitosan-Guargum/Silver blend nanocomposite (CGAgPS) have been synthesised and evaluated for its catalytic activity in degrading individual Reactive and Xanthene dyes and also binary mixture of the dyes. Also the reduction of 4-nitrophenol to 4-aminophenol is also evaluated.

2.5.1 Materials and methods

Chitosan Flakes (Sigma, Medium Mol. Wt.), silver nitrate (Merck, 99.9%), 4-nitrophenol (extrapure AR); commercially used dyes Reactive blue-21(RB-21), Reactive red-141, Rhodamine-6G (RH-6G), hydrogen peroxide (H_2O_2, Fisher Scientific; 30%solution), were used in this study without further purification. AgPS synthesized in section 2.1.2

2.5.2 Synthesis of Silver-Chitosan nanocomposite (CAgPS)

1% Chitosan solution was prepared using acetic acid. To this solution of chitosan the synthesised silver nanoparticle solution was directly added at room temperature and kept in stirring condition for 60 min for uniform dispersion of silver onto chitosan which is then casted in a Teflon plate and kept for drying at 60^0C.

2.5.3 Synthesis of Chitosan-Guargum blend/Silver nanocomposite (CGAgPS)

Chitosan (1%, w/v) was solubilized in 1% (v/v) acetic acid solution while Guargum (1%, w/v) was dissolved in distilled water. To this polymer blend solution the synthesized silver nanoparticle solution was added and kept in stirring condition at room temperature for 1 h.

Characterization studies of CAgPS and CGAgPS were by the instruments and techniques mentioned in section 2.1.3

2.6 Results and discussion

2.6.1 Zeta potential analysis

Figure 2.29 shows the Zeta potential curve for the synthesized nanocomposites CAgPS and CGAgPS at different pHs. At acidic pH the zeta potential is positive (CAgPS: + 63.21mV and CGAgPS: +12.64mV) and from pH 9 the zeta potential values were negative (CAgPS: -24.56 mV and CGAgPS: -28.95mV).

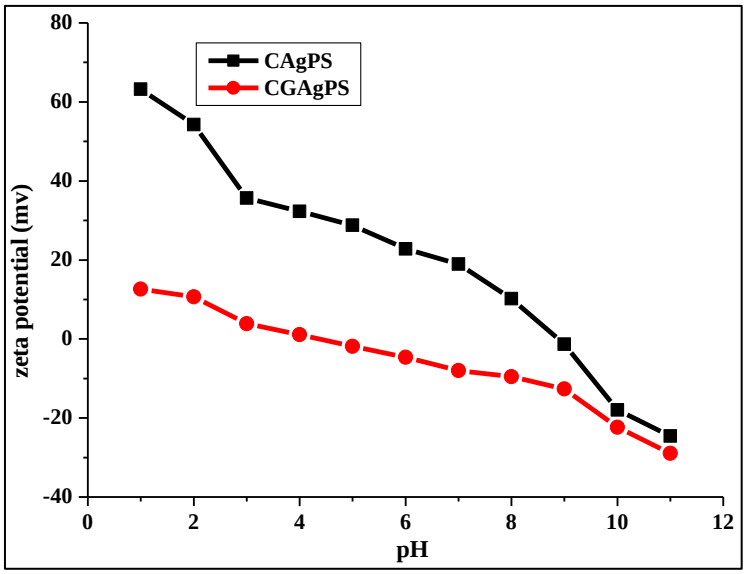

Figure 2.29 Zeta potential spectra of colloidal solution of CAgPS and CGAgPS

2.6.2 Morphology of CAgPS and CGAgPS

Figure 2.30(a) and 2.30(b) shows the TEM imagesof CAgPS and CGAgPS. The TEM micrographs of CAgPS and CGAgPS show that the nanocomposite formed in both the cases are spherical/triangular/Hexagonal/rod like in shape with an average diameter of about 50 - 100 nm in CAgPS and 50 nm in CGAgPS. Figure2.31(a) and 2.31 (b) shows the EDAX spectra of CAgPS and CGAgPS. The presence of the elemental silver in the nanocomposites can be confirmed from EDAX analysis.

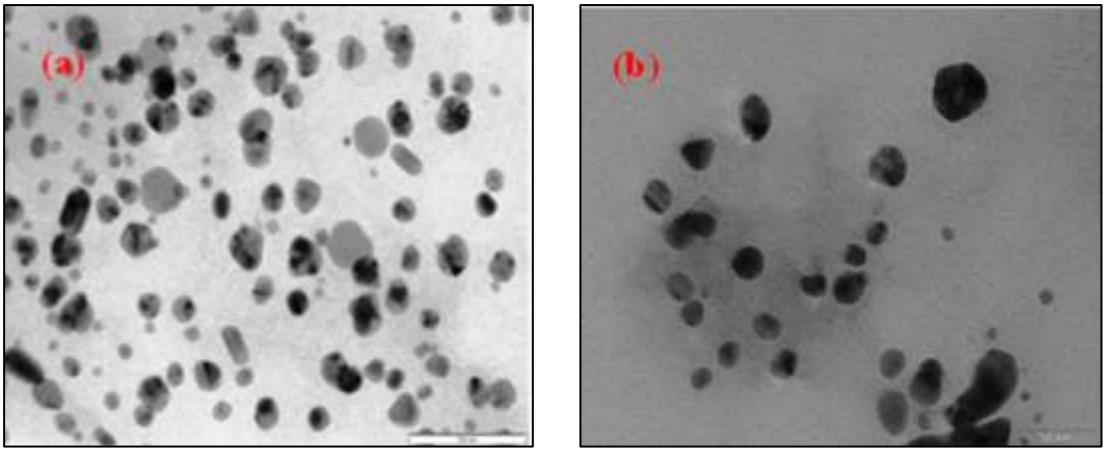

Figure 2.30 TEM morphology images of (a) CAgPS and (b) CGAgS

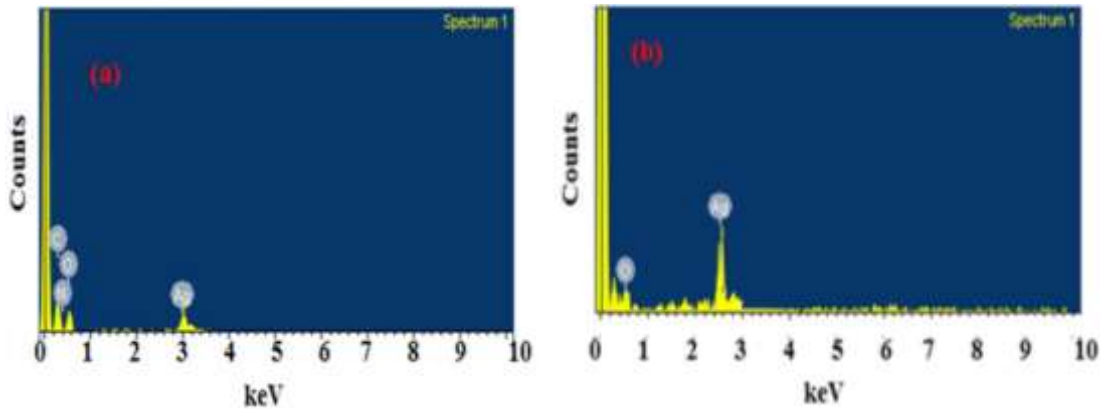

Figure 2.31 EDX images of a) CAgPS and b) CGAgS

2.6.3 FT-IR spectroscopy

Figure 2.32 shows the FT-IR spectrum of Chitosan-Guargum (CG), Chitosan Silver nanocomposite (CAgPS) and Chitosan-Guargum/silver nanocomposite (CGAgPS). Table 2.4 shows the FT-IR stretching frequencies along with their assignments. The peak at 3315 cm^{-1} in CG which is due to the -OH stretching vibration of polymer hydrogen bonding in the polymeric blend. The broad peak observed in the case of CGAgPS and CGS at 3400 and 3407cm^{-1} indicates the presence of -OH group in the nanocomposite and the presence of hydrogen bonding. The peak at 2892 cm^{-1} and 2930 cm^{-1} is due to the -C-H stretching vibration of the –CH_2n. The peak at 1590 cm^{-1} in the case of CAgPS can be attributed to stretching vibration of –N-H in plane bending while the weak intensity peak at 1752 cm^{-1} is attributed to carbonyl group. The peak at 1155 cm^{-1} in the case of CG can be attributed to C–C stretching vibration and asymmetric C–H bending of CH_2 groups of

chitosan moiety. The peak at 1642cm^{-1} in CGS and the peak at 1529 cm^{-1} in CG are due the amide-I and amide-II bands of chitosan matrix involved in the blend formation [133]. The peak around 610 cm^{-1} and 617 cm^{-1} in the case of CAgPS and CGAgPS respectively clearly specifies the presence of metal-oxygen bond involvement in both the nanocomposites.

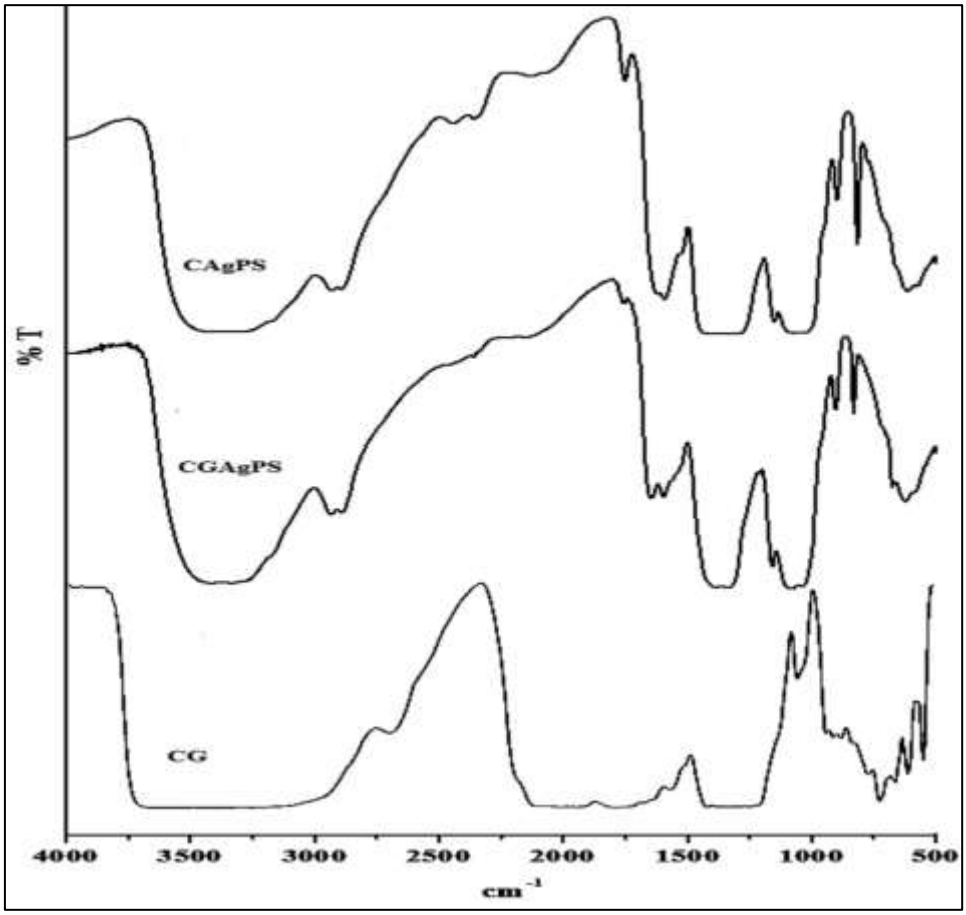

Figure 2.32 FT-IR spectrum of chitosan-guargum blend (CG), Chitosan Silver nanocomposite (CAgPS) and Chitosan-Guargum/silver nanocomposite (CGAgPS)

Table 2.4 FT-IR stretching frequencies

CG	**CAgPS**	**CGAgPS**	**Inference**
3315	3400	3407	-OH stretching vibration
2146	2932	2930	–C-H stretching vibration of the –CH_2group
	1752		carbonyl group stretching
1642,529	1590	1642	amide-1 and amide-11 bands of Chitosan matrix
1155	1073	1022	C–C stretching vibration and asymmetric C–H bending of CH_2 group
770	610	617	Metal-oxygen bonding

2.6.4 X-Ray diffraction studies

The XRD pattern of CG, CGAgPS and CAgPS is shown in Figure2.33,2.34 and 2.36. The peaks at 2θ values 9.3^0 and 13.52^0 observed for CAgPS are due to the Chitosan matrix involved in the nanocomposite. The diffraction peaks of silver in CAgPS were obtained at 2θ values of 38.73, 40.68, 64.67 and 76.62 which corresponds to the (111), (200), (220) and (311) reflection planes of Silver [134].The diffraction peaks of silver in CGAgPS present in the spectra at 2θvalues 35.67, 42.91and 64.33 were indexed to the (111), (220) and (200) reflections. Furthermore, the x-ray pattern of CG indicates the amorphous nature of the blend [135]. The silver nanoparticle incorporated into the biopolymer blend corresponds to a face centered cubic phase of metallic silver.

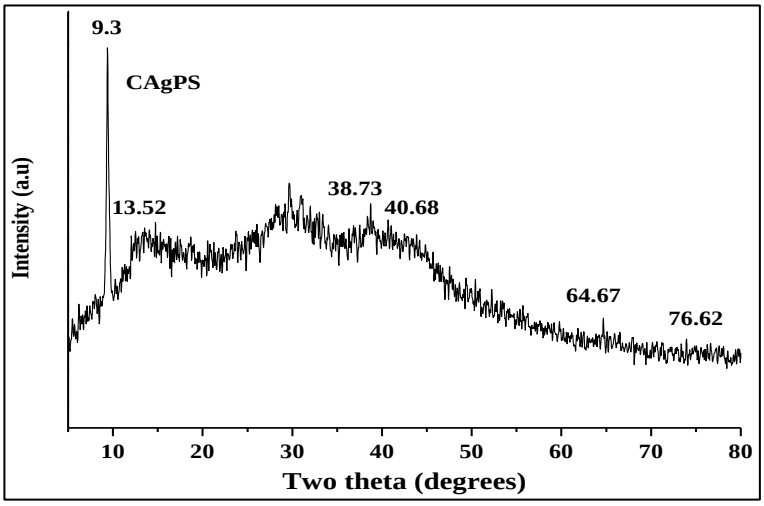

Figure 2.33 X-ray diffraction pattern of CAgPS

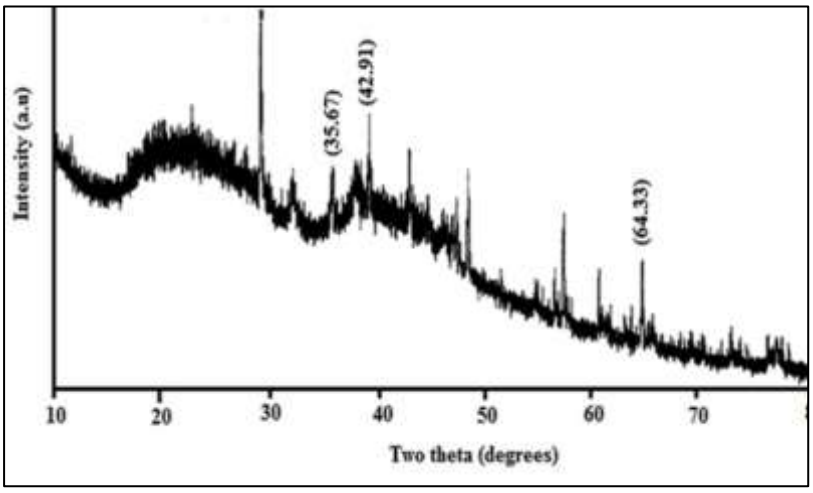

Figure 2.34 X-ray diffraction patterns of CGAgPS

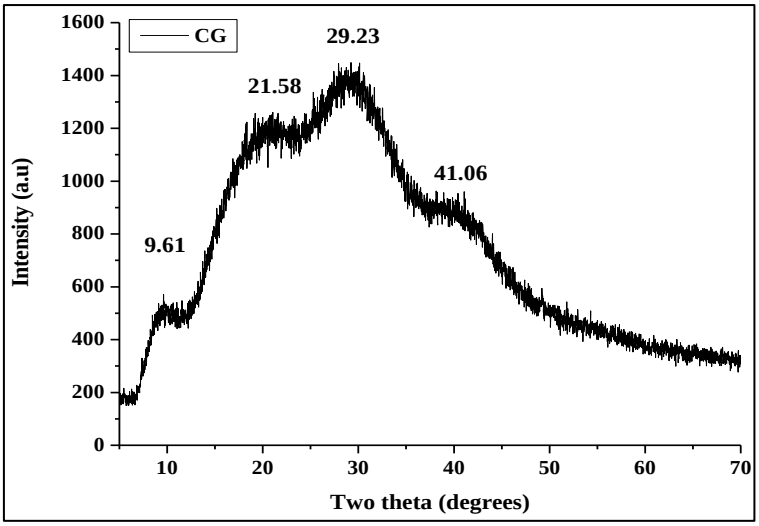

Figure 2.35 X-ray diffraction pattern of CG

2.6.5 Raman spectroscopy studies

Figure 2.36shows the Raman spectra of CAgPS and CGAgPS. The peak at 237 cm^{-1} is attributed to stretching vibration of Ag-N and Ag-O bonds which indicates the interaction of silver with the amino groups and the carboxylate groups of chitosan [97,96]. The peaks at 1344 cm^{-1} and 1598 cm^{-1}were assigned to symmetrical and asymmetrical C=O stretching vibrations respectively. The peak at 897 cm^{-1} and 818 cm^{-1} for CAgPS and CGAgPS can be attributed to the C–H in plane bending and out of plane wag of the biopolymeric matrix. The peak at 2708 cm^{-1} of CAgPS is attributed to the symmetric -C-H stretching frequency associated with the chitosan matrix. The peaks at 1315 and 1518 cm^{-1} correspond to symmetric and asymmetric C=O stretching vibrations of carboxylate group. The peak at 1043 cm^{-1} is attributed to C-H bending frequency.

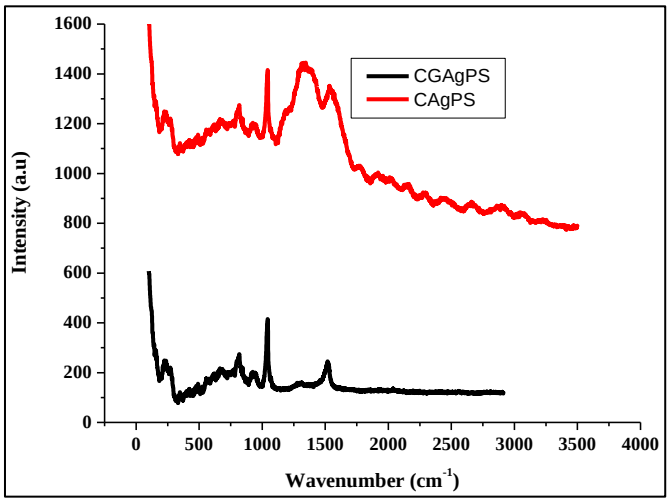

Figure 2.36 Raman spectra of CAgPS and CGS

Figure 2.37 shows the Raman spectra of RB-21, CAgPS-RB and CGAgPS-RB. The peaks observed for RB-21 , CAgPSRB and CGAgPS at 613 cm^{-1} and 647 cm^{-1} are assigned to out of plane C-H bending which has been shifted to 757 $cm^{-1}$and 798 cm^{-1} respectively after loading of the phthalocyanine dye onto CGAgPS-RB.. The peaks of at 1367 cm^{-1},1362 cm^{-1} and 1599 cm^{-1},1598 cm^{-1} in CAgPS-RB and CGAgPS-RB are assigned to the symmetrical and asymmetrical C=O stretching vibrations respectively [136]. The peak at 897 cm^{-1} can be attributed to the C–H in plane bending and out of plane wag of chitosan. There is a shift in C-H stretching frequency from 2762 cm^{-1} to 2845cm^{-1} which might be due to the interaction of the dye molecule with CAgPS. Also, it was observed that after loading of the phthalocyanine moiety to the nanocomposites the symmetrical and asymmetrical stretching frequencies have been shifted to longer wavelength which might be due to the energy loss during molecular transition from ground state to excited state on exposure to laser radiation. It was observed that SERS enhancement was around two times for CAgPS-RR and 5 times for CGAgPS-RR.

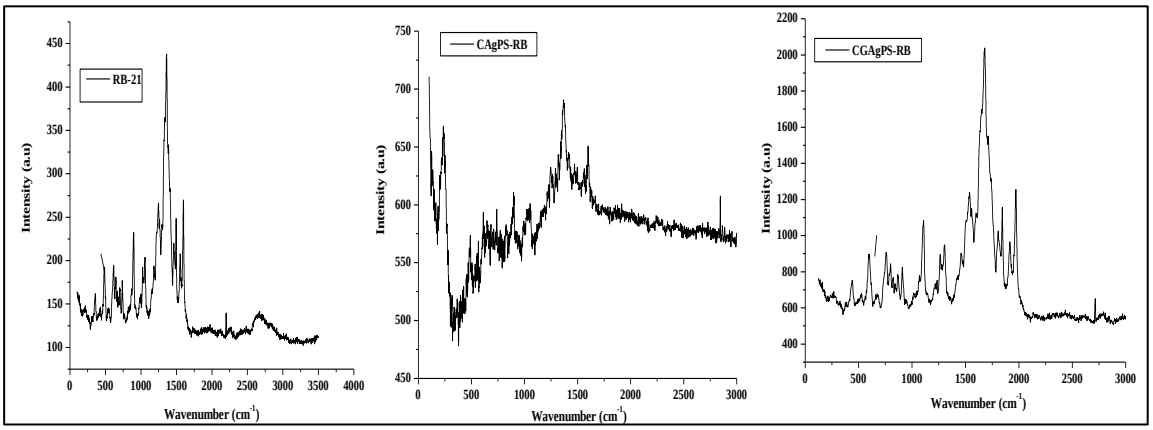

Figure 2.3.7 Raman spectra of RB-21,CAgPS-RB and CGAgPS-RB

Figure 2.38, shows the Raman spectra of RR-141,CAgPS-RR and CGAgPS-RR. The strong interaction of the dye molecule with the catalyst has made a shift of the peaks with increase in intensity [137]. The peaks at 1008 cm^{-1} and 1285 cm^{-1} are attributed to C-C stretching and N=N stretching vibrations respectively for RR. After adsorption the C-C stretching frequency at 1008 cm^{-1} had disappeared and the peak at 1651 $cm^{-1}$of CAgPS and CGAgPS which is attributed to C=O stretching have been shifted to 1594and 1587 cm^{-1}after adsorption with an enhancement in intensity.After loading of the dye the Raman intensity has increased 6 X 10^2 times which shows the SERS enhancement of the azo dye molecule using CGAgPS substrate.

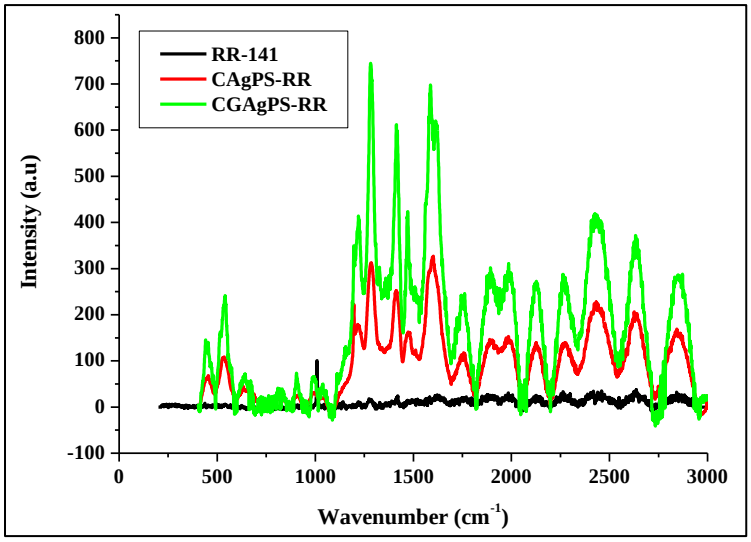

Figure 2.38 Raman spectra of RR-141,CAgPS-RR and CGAgPS-RR

Figure 2.39 shows the Raman spectra of CAgPS-RH and CGAgPS-RH. The bands at 612, 771 and 1182 cm^{-1} in CAgPS and the bands at 525,799 and 1132 cm^{-1} for CGAgPS could be assigned to C–C–C ring in-plane bending, out-of-plane bending motion of the hydrogen atoms of the xanthene skeleton, and C–H stretching vibrations, respectively, while the bands at 1364, 1509 and 1651 cm^{-1} were attributed to the aromatic C–C stretching vibrations of Rh6G molecules [138]. It was observed that after loading Rh6G onto the catalyst the SERS intensities of CAgPS-RH and CGAgPS-RH was greater than those observed in only Rh6G as reported in literature. This enhancement for the Raman intensity can be due to the absorption of the dye molecule as well due to a specific interaction between the molecule and the surface of the catalyst [139].

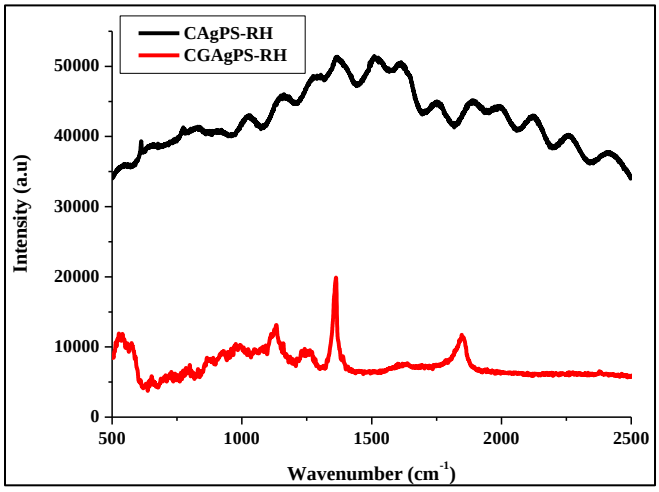

Figure 2.39 Raman spectra of CAgPS-RH and CGAgPS-RH

2.6.6 Degradation studies of individual and binary mixture of dyes

Figures2.40, 2.41, 2.42 and 2.43showed the UV spectra for dye degradation of individual and binary mixture of dyes. The degradation studies were investigated with time using 200 μL of 30% hydrogen peroxide with CAgPS and CGAgPS as a catalyst. The initial concentration of RB-21, RR-141, Rh6G and mixture of dyes was 100 mg/L. Degradation of the dyes did not occur in the presence of only30%H_2O_2. However, complete degradation of RB- 21 occurred within 15 minutes and 2 min in the presence of CAgPS and CGAgPS respectively. In the case of RR-141 it took 6 min. and 15 min using CAgPS and CGAgPS respectively for 95% degradation while for Rh6G 60% degradation occurred within 30 mins using CAgPS and 5 min for 90% degradation using CGAgPS as a catalyst. In the case of mixture of dyes using CAgPS it was observed that in the mixture (RB+RR) complete degradation of RB took place within few minutes while 96 percent RR degraded within 20 min. In the case of RR+RH after 15 min., 80% of the dye mixture has been degraded after which further degradation did not take place even after keeping for a longer time.In the case of mixture of dyes using CGAgPS, 95 % degradation was observed in RB+RH, complete degradation in RR+RH and 90 % degradation in RB+RR binary mixtures. The fast degradation rate of individual and mixture of dyes might be due to the smaller particle size in CGAgPS because smaller the size there would be an increase in specific area of the particles of the nanocomposite which increases the rate of degradation. During the degradation process, it was observed that the characteristic absorption of the particular dye decreases and almost it disappears during the process of degradation which indicates that the chromophore and conjugated system is destroyed. The recycling efficiency of the catalyst was tested by recycling the catalyst. After each run, the catalyst was carefully separated from the solution, and then washed with water. The above catalytic process was repeated for 3 cycles (Figure 2.44) for individual and mixture of dyes. After 3 cycle of catalytic process it was that observed that efficiency decreased within 2-3% and this indicates efficient reusability of the catalyst.

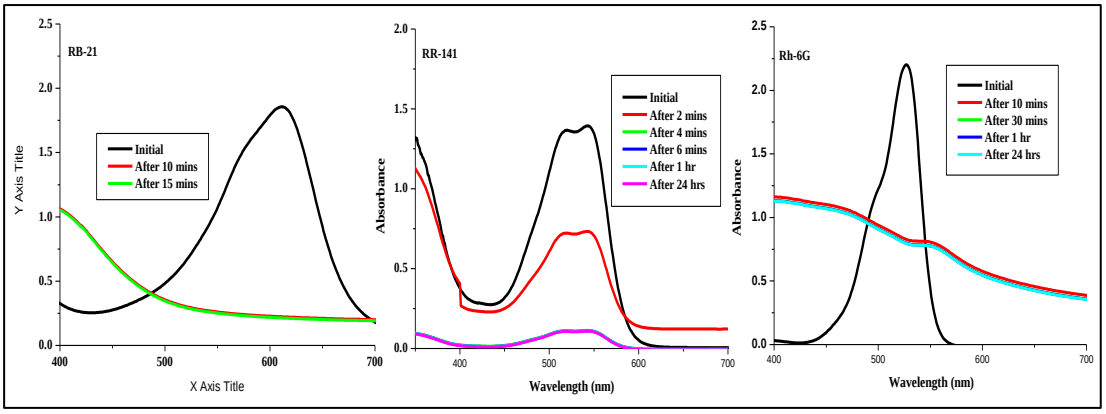

pH 6; RT; Concentration 100 ppm, 3 ml; 0.5 mg catalyst; 200 µL H_2O_2

Figure 2.40 Degradation studies of RB-21, RR-141 and Rh-6G using CAgPS as a catalyst

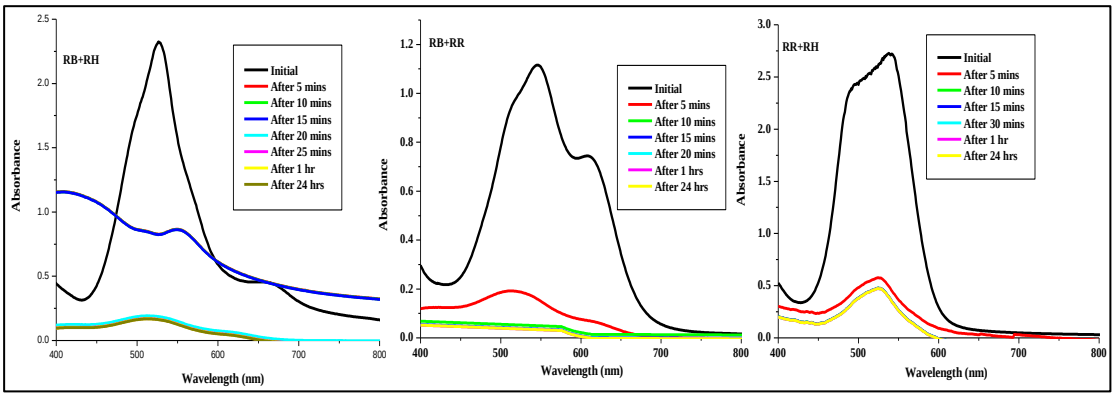

pH 6; RT; Concentration 100 ppm, 3 ml; 0.5 mg catalyst; 200 µL H_2O_2

Figure 2.41 Degradation studies of RB+RH, RB+RR and RR+RH using CAgPS as a catalyst

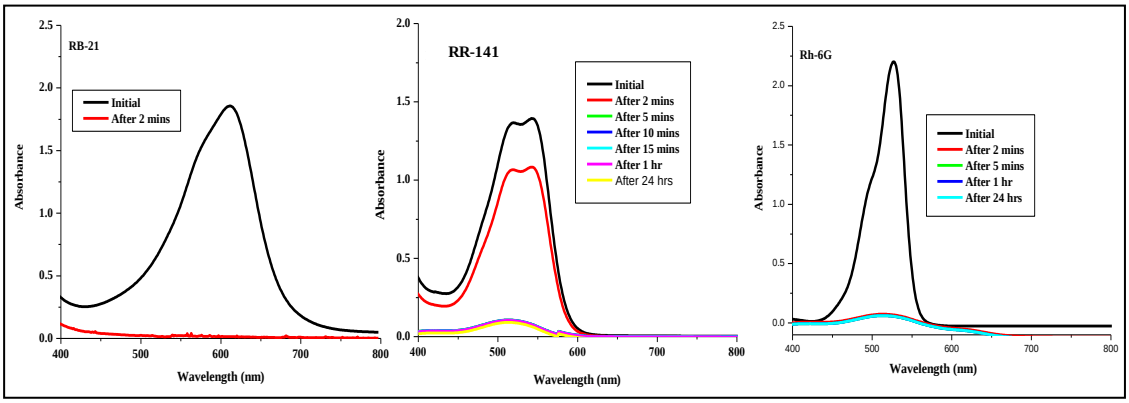

pH 6; RT; Concentration 100 ppm, 3 ml; 0.5 mg catalyst; 200 µL H_2O_2

Figure 2.42 Degradation studies of RB-21, RR-141 and Rh-6G using CGAgPS as a catalyst

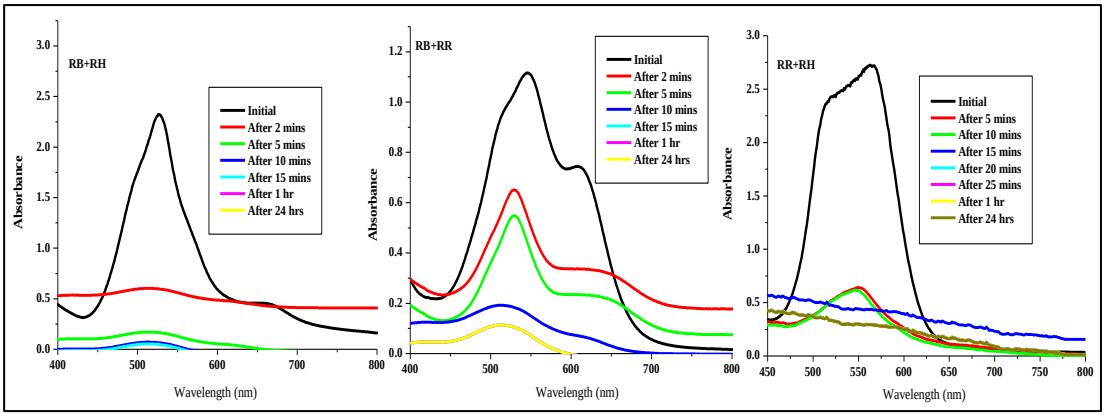

pH 6; RT; Concentration 100 ppm, 3 ml; 0.5 mg catalyst; 200 µL H_2O_2

Figure 2.43 Degradation studies of RB+RH, RB+RR and RR+RH using CGAgPS as a catalyst

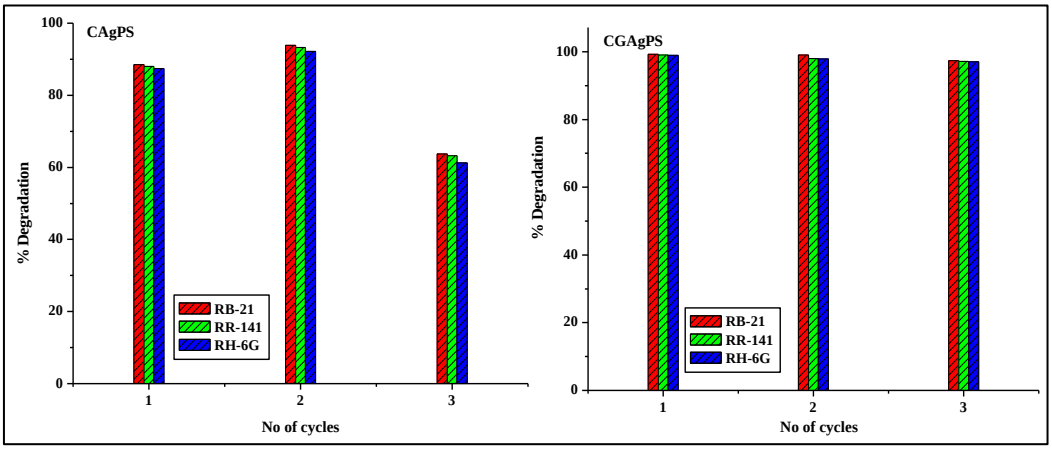

Figure 2.44 Catalyst reusability studies of RB-21, RR-141 and Rh-6G using AgPS, CAgPS and CGAgPS as a catalyst

2.6.7 Total organic content

The mineralization of organic carbon of the dyes in single component systems and binary components was investigated by the Total Organic Carbon (TOC) measurement which has been represented in Figure 2.45. It was observed that there was 77, 50 and 59% reduction in TOC for RB-21, RR-141 and Rh6G respectively for CAgPS in single component systems and 60, 52 and 72% for RB+RH, RR+RH and RB+RR binary systems respectively. In the case of CGAgPS the TOC reduction was 82, 63 and 71% for single component systems comprising RB-21, RR-141 and Rh6G respectively and 65, 57 and 78% for RB+RH, RR+RH and RB+RR binary systems. The TOC reduction is lesser than decolorization which may be due to the formation of smaller colourless products.

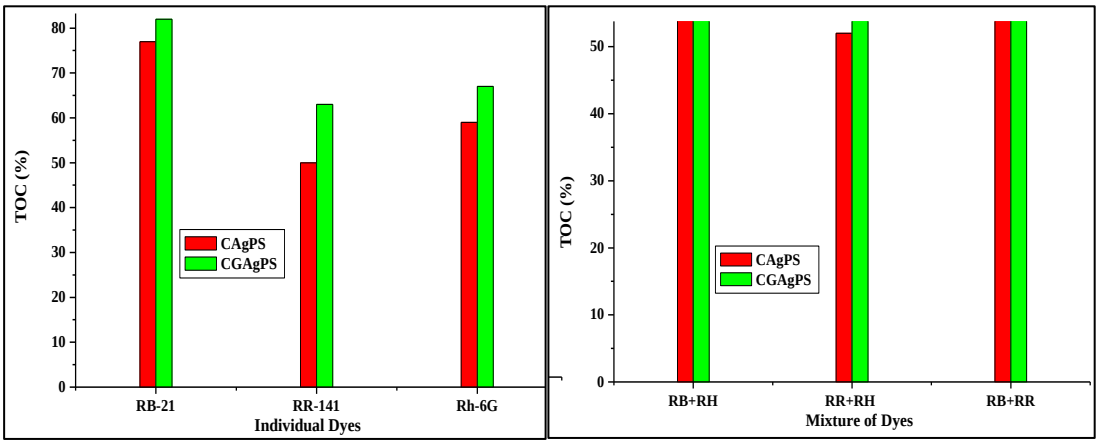

Figure 2.45 Total organic content of degraded dyes

2.6.8 Catalytic reduction of p-nitrophenol

The catalytic properties of the CAgPS and CGAgPS were examined for the reduction of pollutant p-nitrophenol in the presence of sodium borohydride. The absorption spectra of the reduction of 4-nitrophenol catalysed by CAgPS and CGAgPS is shown in Figure 2.46. The reduction reaction of 4-nitrophenol was initiated, as soon as the catalyst was added into 4-nitrophenol. It was observed that the intensity of 401 nm band of p-nitrophenol decreased, with the simultaneous appearance of a new band at 298 nm, corresponding to the formation of 4-aminophenol in the solution. It was observed that 98% and 86% reduction of NP occurred using CAgPS and CGAgPS respectively. The catalyst was efficient upto 3 cycles.

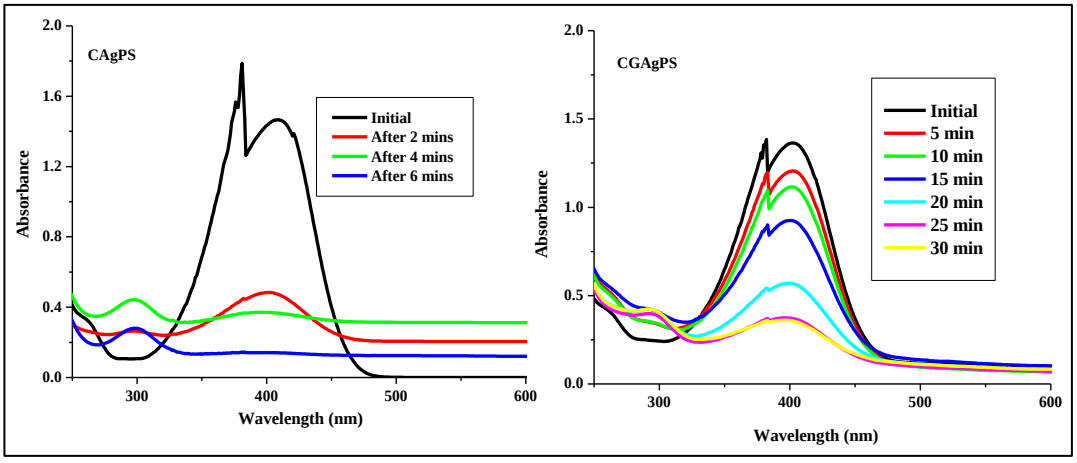

Figure 2.46 Reduction of 4-nitrophenol using CAgPS and CGAgPS as catalyst

2.6.9 Discussion

The catalytic action of Ag nanoparticles could be due to multiple mechanisms. It is possible that the reaction between AgNPs and H_2O_2results in the formation of a highly oxidizing intermediate, such as the hydroxyl radical or some form of Ag-H_2O_2 species, in a manner analogous to the reaction between ferrous iron and H_2O_2 (i.e., a "silver-Fenton reaction") [84, 140]

$$AgNP + H_2O_2 \longrightarrow \text{Intermediate}$$

Furthermore, in the presence of silver, hydrogen peroxide undergoes a heterogeneous catalytic process decomposing to water and oxygen. Firstly, generation of surface silver hydroxide and hydroxyl radicals occurs on the silver surface. Hydroxyl radicals then react with H_2O_2 to form H_2O and $HO_2^{\bullet}$ radicals and $AgOH_{surface}$ reacts with either H_2O_2 or $HO_2^{\bullet}$, regenerating the silver metal surface which enhance the catalytic degradation of dyes [adopted from141].

$$\mathbf{2H_2O_2 \xrightarrow{Ag} 2H_2O + O_2}$$

$$\mathbf{Ag + H_2O_2 \rightarrow AgOH_{surf} + OH^{\bullet}}$$

$$\mathbf{OH^{\bullet} + H_2O_2 \rightarrow H_2O + HO_2^{\bullet}}$$

$$\mathbf{AgOH_{surf} + HO_2^{\bullet} \rightarrow Ag + H_2O + O_2}$$

Previous studies have demonstrated the production of O2$^{\bullet-}$ following the reaction of AgNPs with H_2O_2 [83-85, 160] according to the reaction proposed in following equation.

$$\mathbf{Ag^0 + 2H_2O_2 \rightarrow Ag^+ + O_2^{\bullet-} + 2H_2O}$$

The reduction of Ag by O2•- and subsequent reformation of AgNPs is thought to be responsible for the ability of AgNPs to catalytically degrade H_2O_2 [105,142]. According to Jones et al. [105] and He et al [106], $O_2^{\bullet-}$ transfers electrons to the AgNPs, resulting in the formation of highly reactively "charged" nanoparticles. These charged particles subsequently induce the reduction of both $O_2^{\bullet-}$ and Ag^+, resulting in the reformation of AgNPs

$$\mathbf{AgNP + O_2^{\bullet-} \rightarrow AgNP^{*-} + O_2}$$

$$\mathbf{AgNP^{*-} + O_2 \rightarrow AgNP + O_2^{\bullet-}}$$

$$\mathbf{AgNP^{*-} + Ag^+ \rightarrow AgNP + AgNP}$$

It therefore appears that a "complex interplay" amongAgNPs, Ag+, superoxide, hydroxyl and H_2O_2 results in the degradation of dyes [84].

The silver nanoparticles under study showed significant SERS enhancement, especially for Rh-6G. **SERS** signals achieved using nanoparticle clusters can be very strong because of the so-called hot spots generated within the nanoparticle gaps [143-147]. Typically, the enhancement observed from nanoparticle clusters is many orders of magnitude greater than that of single nanoparticles, which can be attributed to plasmon coupling between adjacent nanoparticles within the clusters, resulting in huge electromagnetic field enhancements at junction sites or SERS hotspots [147]. Azo-dyes are characterized by nitrogen to nitrogen double bonds(N= N). The color of azo-dyes is determined by the azo bonds and their associated chromophores and auxochromes. Azo bonds are the most active bonds in azo-dye molecules and can be oxidized by positive hole or hydroxyl radical or reduced by electron in the conduction band. The cleavage of N= N bonds leads to the decoloration of dyes. Looking into the Z_{pc} of the nanoparticles under study which is negative except for CGAgPS the possibility of RR-141 and RB-121 getting adsorbed is lesser.

Inspite of this, degradation of RR-141 and RB-21 was found to be faster and more efficient than Rh6G in single component and binary component dyes. Our observations suggest that adsorption plays no role on the susceptibility of a dye for degradation. To the best of our knowledge till date there has been no correlation established between structure or class of dye and its susceptibility to degradation. Rauf and Salman Ashraf [104] had tried to establish a correlation and had concluded that xanthene dyes are more difficult to degrade than azo dyes. Our observations also show that Rh6G is the most difficult to degrade. However, in contrast to their observations we have found that adsorption does not play a major role in the degradation process. Rh-6G being a cationic dye could be adsorbed better and also gave better SERS enhancement. However, its degradation proved difficult probably due to its xanthene ring while the degradation of anionic dyes was more effective. The SERS enhancement for anionic dyes was lesser which could be due to their large size. Due to steric effect their interaction with the hot spots could be inhibited.

2.6.10 Conclusion

CGAgPS was more effective in reducing TOC, and decolorisation of dyes. The time taken for decolorisation was also lesser. It has a low negative Z_{pc}value (~-8mV). However it was not effective as SERS substrate though it proved more effective for RR141 than other substrates under study. However CAgPS proved more effective as SERS substrate for Rh6G. Z_{pc} was found to be + 20 mV. Furthermore the

average size of the particles was bigger. It is reported that the aggregates of silver or gold nanoparticles are the best suitable structures for optimal functioning as SERS substrates. According to our observation of TEM; the as-prepared silver microspheres are actually made up of some aggregates of silver nanoparticles [148]. The trenches and voids formed between "silver islands" result in number of "hot spots" [149,150] which could amplify the Raman signal. The SERS amplification was observed significantly of the order of 10^4 only for Rh-6G. This shows that the enhancement is only due to hot spots where the dye could interact. It was independent of surface charge on the nanoparticles and probably dependent on size. However, though there are many literature reports on the use of silver nanoparticles as SERS substrates for copper phtahlocyanine the nanoparticles under study did not give significant SERS enhancement except for AgPS (enhancement of the order of 10^3).However all the nanoparticles under study were effective as catalysts and SERS enhancers for Rh6G and were comparable with other silver nanoparticles reported in literature.

Refrences

[1] X. Ren, X. Meng, D. Chen, F. Tang, J. Jiao, *Biosens. Bioelectron.* 21 **(2005)** 433.

[2] S. Sun, C. B. Murray, D. Weller, L. Folks, A. Moser, *Sci.* 287 **(2000)** 1989.

[3] P. V. Kamat, *J. Phys. Chem. B* 106 **(2002)** 7729.

[4] M. Moreno-Manas, R. Pleixats, *Acc. Chem. Res.* 36(**2003)** 638.

[5] S. R. Kanel, B. Manning, L. Charlet, H. Choi, *Environ. Sci. Technol.* 39 **(2005)** 1291.

[6] J. Cao, D. Elliott, W. Zhang, *J. Nanopart. Res.* 7 *(***2005)** 499.

[7] S. Chen, H. Hsu, C. Li, *J. Nanopart. Res.* 6 **(2004)** 639.

[8] R. W. Gillham, S. F. O. Hannesin, *Ground Water* 32 **(1994)** 958.

[9] Y. Lin, C. Wen, F. Chen, *Sep. Purif. Technol.* 64 (**2008)** 26.

[10] C. B. Wang, W. X. Zhang, *Environ. Sci. Technol.* 31 **(1997)** 2154.

[11] M. Fleishman, P.J. Hendra, A. McQuillan, *Chem. Phys. Lett.* 26 **(1974)** 163.

[12] D.L. Janmaire, R.P. Van Duyne, *J. Electroanal. Chem*. 84 **(1977)** 1.

[13] A.Otto, *J. Raman Spectrosc*. 33 **(2002)** 593.

[14] S. Nie, S.R. Emory, *Science* 275 **(1997)** 1102.

[15] K. Kneipp, H. Kneipp, I. Itzkan, R.R. Dasari, M.S. Feld, *Chem. Rev.* 99 **(1999)** 2957.

[16] M. Futamata, Y. Maruyama, M. Ishkawa, *Vib. Spectrosc.* 30 **(2002)** 17.

[17] W. Ruan, C. Wang, N. Ji, Z. Lu, T. Zhou, B. Zhao, J.R. Lombardi, *Langmuir* 24 **(2008)** 8417.

[18] S. Link, Z.L. Wang, M.A. El-Sayed, *J. Phys. Chem. B* 103 **(1999)** 3529.

[19] C.L. Haynes, R.P. Van Duyne, *J. Phys. Chem. B* 105 **(2001)** 5599.

[20] Y.C. Cao, R. Jin, C.A. Mirkin, *Science* 297 **(2002)** 1536.

[21] K. Kneipp, M. Moskovits, H. Kneipp, in: *Surface-Enhanced Raman Scattering*, Springer, **(2006)** Berlin.

[22] A.M. Michaels, M. Nirmal, L.E. Brus, *J. Am. Chem. Soc*. 121 **(1999)** 9932.

[23] H.H. Wang, C.Y. Liu, S.B. Wu, N.W. Liu, C.Y. Peng, T.H. Chan, C.F. Hsu, J.K. Wang, Y.L. Wang, *Adv. Mater*. 18 **(2006)** 491.

[24] Y. Fang, N.H. Seong, D.D. Dlott, *Science* 321 **(2008)** 388.

[25] W.E. Doering, S. Nie, *J. Phys. Chem. B* 106 **(2002)** 311.

[26] S. Stewart, P. M. Fredericks, *Spectrochim. Acta, Part A* 55 **(1999)** 1641.

[27] R. Wen, Y. Fang, *J. Colloid Interface Sci.* 292 **(2005)** 469.

[28] M.V. Canamares, J.V. Garcia-Ramos, S. Sanchez-Cortes, M. Castillejo, M. Oujja, *J. Colloid Interface Sci.* 326 **(2008)** 103.

[29] P. Mukherjee, A. Ahmad, D. Mandal, S. Senapati, S. R.Sainkar, M. I. Khan, R. Parishcha, P. V. Ajaykumar, M. Alam, R. Kumar, M. Sastry, *Nano Lett.* 1 **(2001)**515.

[30] T. Klaus, R. Joerger, E. Olsson, C. G. Granqvist, *Proc. Natl. Acad. Sci. U.S.A.* 96 (**1999)** 13611.

[31] J. K. Fu, Y. Y. Liu, P. Y. Gu, D. L. Tang, Z. Y. Lin, B. X. Yao, S. Z. Weng, *Acta Phys. Chim. Sin.* 16 (**2000)** 779.

[32] P. Mukherjee, A. Ahmad, D. Mandal, S. Senapati, S. R. Sainkar, M. I. Khan, R. Ramani, R. Parischa, P. V. Ajayakumar, M. Alam, M. Sastry, R. Kumar, *Angew. Chem. Int. Ed.* 40 **(2001)** 3585.

[33] P. Yong, N. A. Rowson, J. P. G. Farr, I. R. Harris, L. E. Macaskie, *Biotechnol. Bioeng.* 80 (**2002)** 369.

[34] W. De Windt, P. Aelterman, W. Verstraete, *Environ. Microbiol.* 7 **(2005)** 314.

[35] D. Rautaray, A. Ahmad, M. Sastry, *J. Am. Chem. Soc.* 125 **(2003)** 14656.

[36] D. Rautaray, A. Ahmad, M. Sastry, *J. Mater. Chem.* 14 **(2004)** 2333.

[37] D. Rautaray, A. Sanyal, S. D. Adyanthaya, A. Ahmad, M. Sastry, *Langmuir*.20 (**2004)** 6827.

[38] V. Bansal, D. Rautaray, A. Ahmad, M. Sastry, *J. Mater.Chem.* 14 **(2004)** 3303.

[39] V. Bansal, D. Rautaray, A. Bharde, K. Ahire, A. Sanyal, A. Ahmad, M. Sastry, *J. Mater. Chem*15**(2005)** 2583.

[40] V. Bansal, A. Ahmad, M. Sastry, *J. Am. Chem. Soc.* 128 **(2006)** 14059.

[41] A. Sanyal, D. Rautaray, V. Bansal, A. Ahmad, M. Sastry, *Langmuir*.21 **(2005)** 7220.

[42] V. Bansal, P. Poddar, A. Ahmad, M. Sastry, *J. Am. Chem. Soc.*128 **(2006)** 11958.

[43] A. K. Jha, K. Prasad, *Colloids Surf. B* 75 **(2010)** 330.

[44] Bharde, D. Rautaray, V. Bansal, A. Ahmad, I. Sarkar, S. M. Yusuf, M. Sanyal, M. Sastry, *Small* 2**(2006)** 135.

[45] Ahmad, T. Jagadale, V. Dhas, S. Khan, S. Patil, R. Pasricha, V. Ravi, S. Ogale, *Adv. Mater.*, 19 **(2007)** 3295.

[46] Ahmad, P. Mukherjee, D. Mandal, S. Senapati, M. I. Khan, R. Kumar, M. Sastry, *J. Am. Chem. Soc.* 12 **(2002)** 12108.

[47] S. H. Kang, K. N. Bozhilov, N. V. Myung, A. Mulchandani, W. Chen, *Angew. Chem., Int. Ed.* 47 **(2008)** 5186.

[48] A. K. Jha, K. Prasad, K. Prasad, *Biochem. Eng. J.* 43 **(2009)** 303.

[49] P. Mohanpuria, N. K. Rana, S. K. Yadav, *J. Nanopart. Res.* 10 **(2008)** 507.

[50] V. Kumar, S. K. Yadav, *J. Chem. Technol. Biotechnol.* 84 **(2009)** 151.

[51] J. L. Torresdey, E. Gomez, J. R. Videa, J. G. Parsons, H. Troiani, M. J. Yacaman, *Langmuir* 19 (**2003)** 1357.

[52] S. S. Shankar, A. Ahmad, M. Sastry, *Biotechnol. Prog.*, 19 **(2003)** 1627.

[53] S. S. Shankar, A. Rai, A. Ahmad, M. Sastry, *J. Colloid Interface Sci.* 275 **(2004)**, 496.

[54] Ankamwar, C. Damle, A. Ahmad, M. Sastry, *J. Nanosci. Nanotechnol.* 5 (**2005)** 1665.

[55] S. P. Chandran, M. Chaudhary, R. Pasricha, A. Ahmad, M. Sastry, *Biotechnol. Prog.* 22 **(2006)** 577.

[56] J. P. Xie, J. Y. Lee, D. I. C. Wang, Y. P. Ting, *ACS Nano.* 1 **(2007)** 429.

[57] S. K. Li, Y. H. Shen, A. J. Xie, X. R. Yu, L. G. Qiu, L. Zhang, Q. F. Zhang, *Green Chem*. 9 **(2007)** 852.

[58] M. N. Nadagouda, R. S. Varma, *Green Chem*. 10 **(2008)** 859.

[59] A. R. Nestor, V. S. Mendieta, M. A. C. Lopez, R. M. G. Espinosa, M. A. C. Lopez, J. A. A. Alatorre, *Mater. Lett.* 62 **(2008)** 3103.

[60] K. Jha, K. Prasad, V. Kumar, K. Prasad, *Biotechnol. Prog*., 25 **(2009)** 1476.

[61] T. C. Prathna, N. Chandrasekaran, A. M. Raichur, A. Mukherjee, *Colloids Surf. A* 377 **(2011)** 212.

[62] J. L. Huang, Q. B. Li, D. H. Sun, Y. H. Lu, Y. B. Su, X. Yang, H. X. Wang, Y. P. Wang, W. Y. Shao, N. He, J. Q. Hong, C. X. Chen, *Nanotechnol.* 18 **(2007)** 105104.

[63] J. L. Huang, L. Q. Lin, Q. B. Li, D. H. Sun, Y. P. Wang, Y. H. Lu, N. He, K. Yang, X. Yang, H. X. Wang, W. T. Wang, W. S. Lin, *Ind. Eng. Chem. Res.* 47 **(2008)** 6081.

[64] S. Kushwaha, B. Sreedhar, P. P. Sudhakar, *Bioresour. Technol.* 116 **(2012)** 15.

[65] S. Kushwaha, B. Sreedhar, P. P. Sudhakar, *Chem. Eng. J.* 328 **(2012)** 193.

[66] N. Mude, A. Ingle, A. Gade, M. Rai, *J. Plant Biochem. Biotechnol.*, 18 **(2009)** 83.

[67] M. Yilmaz , H. Turkdemir , M. AkifKilic, E. Bayram, A. Ciceke,, A. Mete, B. Ulugg, *Mat. Chem. Phys.* 130 **(2011)** 1195.

[68] A.J. Kora, R. Manjusha. J. Arunachalam, *Mater. Sci. Eng., C* 29 **(2009)** 2104.

[69] W. J. Cho, Y. Kim and J. K. Kim, *ACS Nano*6 **(2012)** 249.

[70] A. leelavathi, T. U. B. Rao, T. Pradeep, *International Journal of Nanoscience* 10 **(2011)** 839.

[71] Y. M. Mohan, K. M. Raju, K. Sambasivudu, S. Singh, B. Sreedhar, *J. Appl. Polym. Sci.* 106 **(2007)** 3375

[72] S. J. Jun, S. Kim, J.H. Han. *J. Kor. Ceram. Soc.* 35 **(1998)** 209.

[73] M. Sastry, A. Ahmad, M.I. Khan, R. Kumar, *Curr. Sci*. 85 **(2003)** 162.

[74] G. S. S. Saini, S. Kaur, S. K. Tripathi, C. G. Mahajan, H. H. Thanga, A. L. Verma, *Spectrochim. Acta, Part A* 61 **(2005)** 653.

[75] Hildebrant, M. Stockburger, *J. Phys. Chem.* 88 **(1984)** 5935.

[76] L. Y. Chuan, Y. C. Chin, S. S. Fu, *J. Mater. Chem.* 16 **(2006)** 3546.

[77] K. chanderia, S. Kalal, J. Sharma, N. Ameta, P. B. Punjabi, *Indian J. Chem., Sect A*. 52 **(2013)** 1416.

[78] X. Guo, Y. Fu, S. Fu, H. Wang, T. Yang, Y. Wen, H. Yang, *Inorg. Chem.* 53 **(2014)** 7227.

[79] Y. Q. Wang, S. Ma, Q. Q. Yang, X. J. Li, *Appl. Surf. Sci*. 258 (**2012)** 5881.

[80] J. P. Camden, J. A. Dieringer, Y. M. Wang, D. J. Masiello, L. D. Marks, G. C. Schatz, R. P. Van Duyne, *J. Am. Chem. Soc.* 130 **(2008)** 12616.

[81] K. Lim, K. S. Jeon, H. M. Kim, J. M. Nam, Y. D. Suh, *Nat. mater.* 9 (**2010)** 60.

[82] S. Nie, S. R. Emory, *Science* 275 **(1997)** 1102.

[83] T. Endo, Y. Yanagida, T. Hatsuzawa, *Measurement* 41 **(2008)** 1045.

[84] J. Z. Guo, H. Cui, W. Zhou, W. Wang, *J. Photochem. Photobiol., A: Chem.* 193**(2008)** 89.

[85] Y. Ono, T. Matsumura, N. Kitajima, S.-I. Fukurumi, *J. Phys. Chem.* 81**(1977)** 1307.

[86] A. J. Kora, R. B. Sashidhar and J. Arunachalam, *Carbohydr. Polym.* 82 **(2010)** 670.

[87] V. T. P. Vinod, P. Saravanan, B. Sreedhar, D. K. Devi and R. B. Sashidhar, *Colloids Surf. B* 83 **(2011)** 291.

[88] S. Dhar, E. M. Reddy, A. Shiras, V. Pokharkar and B. L. V. Prasad, *Chem. Eur. J.* 14 **(2008)** 10244.

[89] TC-Y. Leung, C. K. Wong and Y. Xie, *Mater. Chem.Phys.* 121 **(2010**) 402.

[90] A. Pal, K. Esumi, T. Pal, *J. Colloid Interface Sci*. 288 (**2005)** 396.

[91] H. Jiang, Z. Chen, H. Cao and Y. Huang, *Analyst*, 137 (**2012)** 5560.

[92] G. J. S. Raid, P. M.Day and R. A. Dixon, in: *Biochemistry of Storage Carbohydrates*, , Eds. Academic Press, (**1985**) 265 London.

[93] B. V. McCleary, A. H. Clark, I. C. M. Dea and D. A. Rees, *Carbohydr. Res.* 92 **(1981)** 269.

[94] E.S. Abdel-Halim, M.H. El-Rafie, Salem S. Al-Deyab, *Carbohydr. Polym.* 85 **(2011)** 692.

[95] J. Kora, R. B.Sashidhar, J.Arunachalam, *Org. Med. Chem.Lett.* 2 **(2012)** 17.

[96] Biswas, Kapoor, Mahal, Mukherjee, *Chem. Phys. Lett.* 444 **(2007)** 338.

[97] J. Chowdhury, M. Ghosh, *J. Colloid Interface Sci.*277 **(2004)** 121.

[98] J.Onuegbu, A. Fu, O. Glembocki, S. Pokes, D. Alexson and C. M. Hosten, *Spectrochim. Acta, Part A.* 79 **(2011)** 456.

[99] P. Hildebrandt and M. Stockburger, *J. Phys. Chem.* 88 **(1984)** 5935.

[100] S. Pandey, G. K. Goswami, K. K. Nanda, *Int. J. Biol. Macromol.* 51 **(2012)** 583.

[101] N. Vigneshwaran, R. P. Nachane, R. H. Balasubramanya, P.V. Varadarajan, *Carbohydr. Res*. 341 **(2006)** 2012.

[102] K. Shameli, M. B. Ahmad, S. D. Jazayeri, S. Sedaghat, P. Shabanzadeh, H. Jahangirian, M. Mahdavi, and Y. Abdollahi, *Int. J. Mol. Sci*. 13 **(2012)** 6639.

[103] Y. Xiong, I. Washio, J. Chen, H. Cai, Z. Y. Li, Y. Xia, *Langmuir*22 **(2006)** 8563.

[104] M.A. Rauf, S. Salman Ashraf, *Chem. Eng. J.* 151 **(2009)** 10.

[105] Adele M. Jones , Shikha Garg , Di He , A. Ninh Pham , and T. David Waite,*Environ. Sci. Technol.* 45 **(2011**) 1428.

[106] He, D.; Jones, A. M.; Garg, S.; Pham, A. N.; Waite, T. D, *J. Phys. Chem.C.* 115 **(2011)** 5461.

[107] Liu, J. Y.; Hurt, R. H, *Environ. Sci. Technol.* 44 **(2010)** 2169.

[108] M. Kong, X. G. Chen, K. Xing, H. J. Park, ,*Int. J. Food Microbiol*. 144 **(2010)** 51.

[109] G. B. Ralston, M. V. Tracey, P. M. Wrench,*Biochim. Biophys. Acta* 93 **(1964)** 653.

[110] S. W. Fang, C. F. Li, D. Y. C. Shih, *J. Food Prot.* 57 **(1994)** 136.

[111] D. Raafat, H. G. Sahl, *Microb. Biotechnol.* 2 **(2009)** 186.

[112] W. Dongwei, S. Wuyong, Q. Weiping, Y. Yongzhong, M. Xiaoyuan, Carbohydr. Res. 344 **(2009)** 2375.

[113] D. Wei, W. Qian, *Colloids Surf. B* 62 **(2008)** 136.

[114] A. Futyra, M. Liskiewicz, V. Sebastian, S. Irusta, M. Arruebo, G. Stochel, A. Kyziol, *ACS Appl. Mater. Interfaces* 7 **(2015)** 1087−1099.

[115] K. Yang, Y. Liu, T. Hsu, M. Juang, *Materials Letters* 64 **(2010)** 497.

[116] Q, Zhang, L. Liu,L. Ren, F. Wang, *J. Appl. Polym. Sci*. 64**(1997)** 212.

[117] W. H Jiang, S. J. Han, *J Polym Sci*. 36**(2000)** 1275.

[118] H. S. Blair, J. Guthrie, T. Law, P. Turkington, *J. Appl. Polym. Sci.* 45**(1992)** 1857.

[119] Y.Kurauchi, T. Yanai, K. Ohga, *Chem. Lett.* 8**(1991)** 1411.

[120] D. Y. Kim, J. A. Ratto, R. B. Blumestein, *Polym. Prepr.* 31**(1991)** 112.

[121] M. M. Amiji, *Biomaterials* 16**(1995)** 593.

[122] V. R. Patel, M. M. Amiji, *ACS Symp. Ser.* 627**(1996)** 209.

[123] E.-A. Hugo, G. B.-G. Juan, C.-S. Francisco, E. V.-C. Jaime,*Biomacromolecules* 8 **(2007)** 1313.

[124] H. Zheng, Y. M. Du, J. H. Yu, R. H. Huang, L. Zhang, *J. Appl.Polym. Sci.* 80 **(2001)** 2558.

[125] M. Miya, R. Iwamoto, S. Mima, *J. Polym. Sci*. 22 **(1984)** 1149.

[126] S. Nakatsuka, A. L. Andrady, *J. Appl. Polym. Sci.* 44 **(1992)** 17.

[127] Y. W.Cho, S. S. Han, S. W. Ko, *Polymer* **2000**, *41*, 2033-2039. The adsorption properties and mechanisms of the chitosan/PVA blend for metal removal have however seldom been studied, *Langmuir, Vol. 18, No. 25, 2002*

[128] A. G. Sullad, L. S. Manjeshwar, T. M. Aminabhavi, *J. Appl. Polym. Sci*. 112 **(2011)** 452.

[129] V.Mutalik, L. S. Manjeshwar, A. Wali, M. Sairam, K. V. S. N. Raju, T. M. Aminabhavi, *Carbohydr. Polym.* 65 **(2006)** 9.

[130] H. Huang, Q. Yuan, X. Yang, *Colloids Surf. B.* 39 **(2004)** 31.

[131] A. Murugadoss, A. Chattopadhyay, *Nanotechnology* 19 **(2008)** 603.

[132] D. Wei, Y. Ye, X. Jia, , C. Yuan, , W. Qian, *Carbohydr. Res*. 345 **(2010)** 74.

[133] G. Z. Kyzas, N. K. Lazaridis, *J. Colloid Interface Sci.* 331 **(2009)** 32.

[134] Jing, L. Qingzhi, Y. Xiaoyan, D. Wang, X. Li, *J. Appl. Polym. Sci.*120 **(2011)** 3180.

[135] D. Mudgil, S. Barak, B. S. Khatkar, *Int. J. Biol. Macromol.*50 **(2012)** 1035.

[136] P. Mukherjee, M. Roy, B. P. Mandal, G. K. Dey, P. K. Mukherjee, J. Ghatak, A. K. Tyagi, S. P. Kale, *Nanotechnology* 19 **(2008)** 075103.

[137] A. K. Mishra, T. Arockiadoss, S. Ramaprabhu, *Chem. Eng. J.* 162 **(2010)** 1026.

[138] J. Onuegbu, A. Fu, O. Glembocki, S. Pokes, D. Alexson, C. M. Hosten, *Spectrochim. Acta, Part A* 79 **(2011)** 456-461.

[139] X. Zhao, B. Zhang, K. Ai, G. Zhang, L. Cao , X. Liu, H. Sun, H. Wang, L. Lu, *J. Mater. Chem.* 19 **(2009)** 5547.

[140] Y. Ono, T. Matsumura, N. Kitajima, S. Fukurumi,, *J. Phys. Chem*. 81 **(1977)** 1307.

[141] Z.-M. Hua, H. Nakatsuji, Surf. Sci.425 (**1999**) 296.

[142] A. M. Jones, S. Garg, D. He, A. N. Pham, T. D. Waite, *Environ. Sci. Technol.* 45 **(2011)** 1428.

[143] M. Fleischmann, P. J. Hendra, A. McQuilla, *Chem. Phys. Lett.* 26 **(1974)** 163.

[144] D. L. Jeanmaire, R. P. Van Duyne, *J. Electroanal. Chem.*, 84 **(1977)** 1.

[145] P. Shaw, M. Fan, C. Lane, G. Barry, A. I. Jirasek, A. G. Brolo, *J. Phys. Chem. C* 117 **(2013)** 16596.

[146] J. Ye, F. Wen, H. Sobhani, J. B. Lassiter, P. Van Dorpe, P. Nordlander, N. J. Halas, *Nano Lett.* 12 **(2012)** 1660.

[147] J. C. Fraire, L. A. Perez, E. A. Coronado, *J. Phys. Chem. C* 117 **(2013)** 23090.

[148] D.-P. Yang, S. Chen, P. Huang, X. Wang, W. Jiang, O. Pandoli, D. Cui, Green. *Chem.*12 **(2010)** 2038.

[149] S. M. Nie and S. R. Emery, *Science*, 275 **(1997)** 1102.

[150] S. Eustis and M. A. El-Sayed, *Chem. Soc. Rev.*, 35 **(2006)** 209.